UCRL-17171

University of California

Ernest O. Lawrence Radiation Laboratory

GASEOUS THERMAL ELECTRON REACTIONS

Berkeley, California

DISCLAIMER

UCRL-17171

UNIVERSITY OF CALIFORNIA

Lawrence Radiation Laboratory
Berkeley, California

AEC Contract No. W-7405-eng-48

GASEOUS THERMAL ELECTRON REACTIONS

Charles E. Young

(Ph.D. Thesis)

September 1966

TABLE OF CONTENTS

GASEOUS THERMAL ELECTRON REACTIONS

Charles E. Young

Inorganic Materials Research Division, Lawrence Radiation Laboratory,
and Department of Chemistry
University of California, Berkeley, California

ABSTRACT

We have employed a microwave cavity resonance technique to study the rate of disappearance of gaseous electrons in the presence of molecules which can capture them to form negative ions. Electron concentrations of 10^7 to 10^8 per cc were produced by photoionization of a small amount of NO with a single pulse of 1216Å or 1236Å light from microwave discharge in hydrogen or krypton, respectively. Experimental conditions also involved the presence of 1 to 100 torr of inert gas, which permitted the electrons to reach quickly a Maxwellian energy distribution corresponding to 300°K, and reduced the diffusional loss of electrons.

Under these conditions, electron attachment to SF_6, C_7F_{14} and C_3F_8 was observed to correspond to a two body process with rate constants of 2.7×10^{-7}, 8.8×10^{-8} and 8.8×10^{-12} cc/molecule-sec, respectively. Attachment to C_2F_4 and SiF_4 appeared to be a three body process but estimation of rate constants was less accurate.

The effectiveness of various inert gas molecules in producing three body attachment of electrons to NO was also investigated. For He, Ne, N_2, Ar, Kr and Xe, measured three body rate constants were, respectively, 2.2×10^{-32}, 1.8×10^{-32}, 3.7×10^{-32}, 3.2×10^{-32}, 0.65×10^{-32} and 10.3×10^{-32} $(cc/molecule)^2\ sec^{-1}$.

Analysis of the data required us to correct for ambipolar diffusion but not for ion-electron recombination. A short computer study simulating

the conditions for our experiments on attachment to SF_6 and C_7F_{14} was useful in determining the error involved in estimating attachment rates from electron decay curves.

1. INTRODUCTION

The processes by which electrons may be captured in weakly ionized gases are of considerable practical and theoretical importance. Such processes are important in the earth's ionosphere, to take one example of an area receiving considerable attention at present. It is often more convenient and illuminating to study gaseous electron capture in the laboratory where, hopefully, experimental conditions can be chosen so that a single process of interest predominates.

In the past, in studies of low energy electron capture by neutral molecules, electron beam and drift tube methods have been used most often. In electron beam work, the retarding potential difference technique[1] has achieved energy resolution of .1 to .2 eV, which is still objectionably wide for studying narrow resonant capture processes. In addition, a reliable calibration of the energy scale is hard to achieve. In drift tube methods, the electrons move under the influence of an applied electric field. A variation of this method[2] has permitted the use of an electric field small enough for the electrons to be near thermal energy. In either the electron beam or the drift tube technique, the energy distribution of the electrons is non-Maxwellian.[3,4]

The microwave cavity method used in our research was originally developed by Biondi and Brown at MIT.[5] It has the advantage that the microwave probing signal power can be kept low enough so that the thermal Maxwellian distribution of the electrons is undisturbed. If desired, signal power can be increased, which should simply raise the effective temperature of the electron energy distribution.[6] The usefulness of the microwave method for observing thermal electron attachment was demonstrated

by Biondi[7] in a study of the process $I_2 + e \rightarrow I^- + I$.

Our experimental program divides into two sections. First we studied the rate of attachment of thermal electrons to the fluorine compounds SF_6, C_7F_{14}, C_3F_8, C_2F_4, and SiF_4. This study increased the estimate of the attachment cross sections for SF_6 and C_7F_{14} as well as giving information about the rate and mechanism of attachment to the smaller fluorine compounds. The second part of our program comprised studies of the relative efficiencies of various inert gases in producing three body attachment to NO. These results are discussed in Chapter 5. Earlier chapters describe various aspects of the experimental technique and data analysis.

2. EXPERIMENTAL

A general view of the apparatus is given in Fig. 1. Details concerning various components will be given in later sections. The electron attachment reactions being studied take place in the reaction cell contained in the detection cavity. The gaseous system being studied is loaded into the reaction cell by means of a conventional gas handling system. At the instant that electrons are produced in the reaction cell by photoionizing radiation from the pulsed lamp, a single sweep on the oscilloscope is triggered and a continuous record of free electron concentration vs time is obtained on the CRT. This is photographed with a Polaroid camera for later analysis.

2.I Gases and Handling Procedure

The gas handling system, shown in Fig. 2, was constructed of Pyrex glass. A mercury diffusion pump with liquid nitrogen trap, backed by a conventional rotary mechanical pump produced vacuums of better than 10^{-6} torr. Stopcocks were greased with Apiezon N and when new grease had been outgassed sufficiently, the system showed a pressure-rise rate of about 3×10^{-6} torr per hour when isolated from the pumps. Two mercury McLeod gauges were available for pressure measurements given by

$$\text{Gauge (1)} \qquad p = 3.14\times10^{-6}\ x^2$$

$$\text{Gauge (2)} \qquad p = 1.45\times10^{-4}\ x^2$$

where p is in torr and x is in m.m.

In addition there was a mercury manometer for measuring pressures above a few torr. Ball joint connectors provided a means for attaching to the system various pyrex flasks of gas for use in filling the lamp or reaction cell.

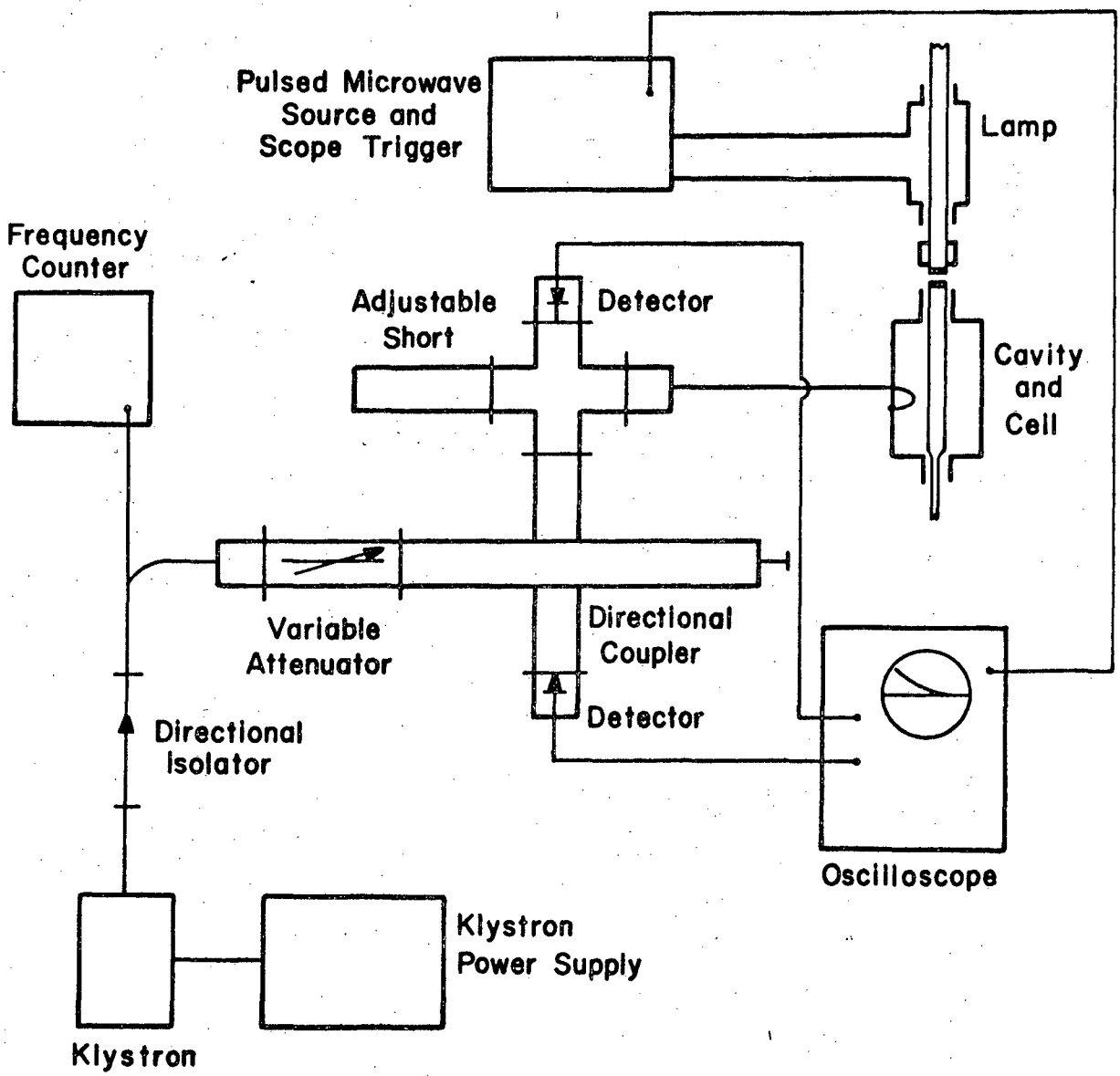

Fig. 1 Block diagram of apparatus

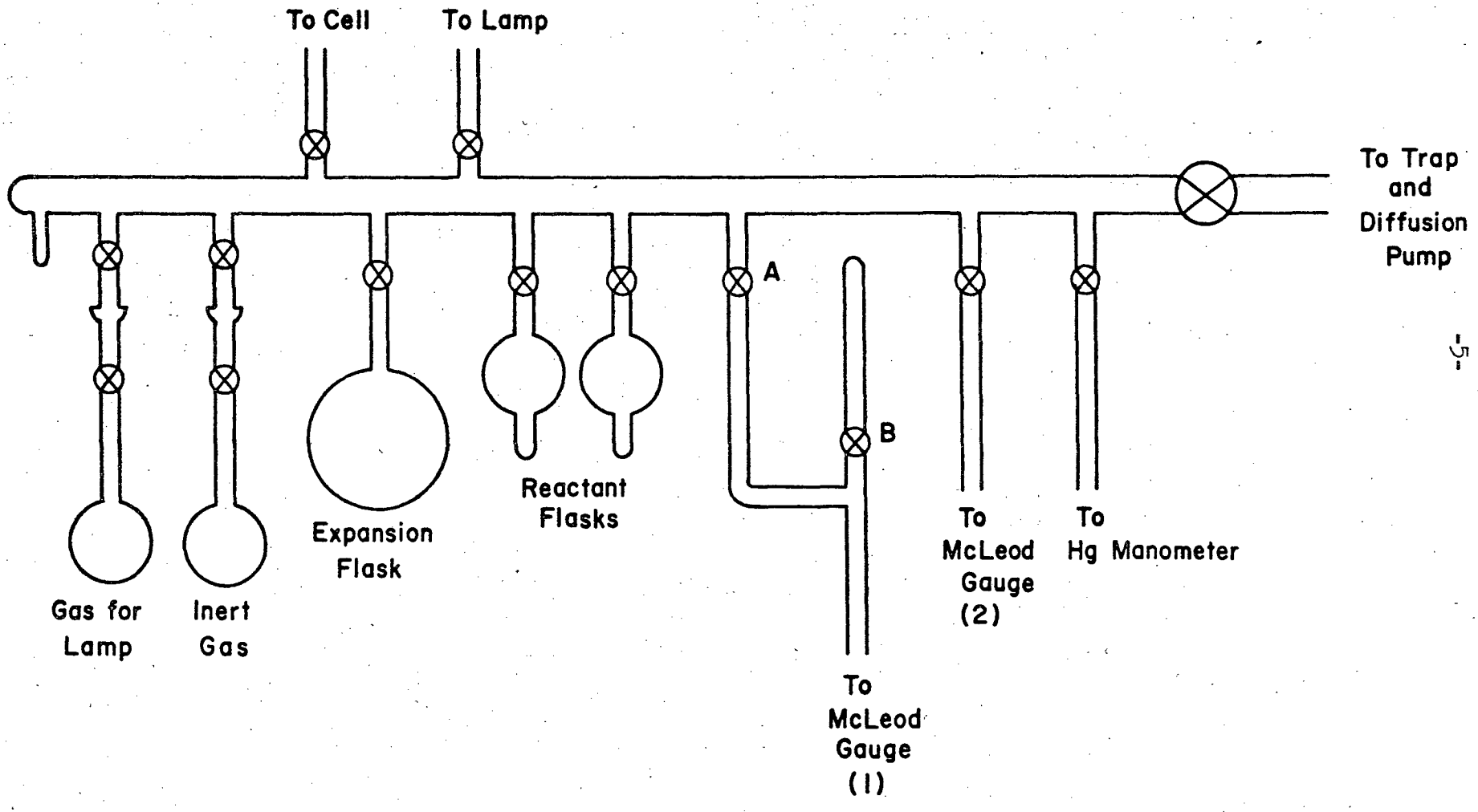

Fig. 2 Vacuum line

The NO used in these experiments was cylinder grade and traces of NO_2 present had to be removed. A removable flask containing NO and NO_2 frozen out at liquid oxygen temperature (-183°C) was attached to the vacuum line by a ball-socket joint and NO was distilled into the trap of a reactant flask, the trap being maintained at liquid nitrogen temperature (-196°C). NO_2 has a negligible vapor pressure at -183°C and remains behind in the trap as do traces of N_2O, N_2O_3 or N_2O_5 which may be present.[8] The contents of the -183°C trap were removed by auxillary roughing pump to avoid contact between NO_2 and mercury in the main vacuum line. Distillation of NO was repeated at least 3 times with initial and final portions discarded. In addition, NO was frozen out at -196°C and pumped on several times for periods of a few minutes. After this preparation, small amounts of NO solid had a pale blue color and conformed within the accuracy of the gauges to the expected vapor pressure at -196°C.[9]

Commercially obtained in lecture bottles were SF_6 from Matheson and C_3F_8 and C_2F_4 from Peninsular Chem Research. The C_7F_{14} used was kindly supplied to us by Professor Joel Hildebrand. SiF_4 was prepared by heating K_2SiF_6 under vacuum and collecting the gas given off.* Before each of the above gases was studied in attachment experiments, it was distilled from an appropriate low-temperature bath into a reactant flask on the main vacuum line.

Inert gases used were reagent grade obtained from Airco or Linde in one-liter pyrex flasks with "breakoffsky" seals. Hydrogen used in the lamp was cylinder grade.

---

* A mass spectrum of this gas was run showing a strong SiF_3^+ peak indicating that the gas was mainly SiF_4. Traces of O_2, N_2 and possibly CO_2 were present.

2.II Reaction Cell Loading Procedure

The large attachement cross sections of SF_6 and C_7F_{14} necessitated the use and measurement of pressures of the order of 10^{-6} torr. To accomplish this a small closed vessel was attached to McLeod gauge (1) through stopcock B (Fig. 2). A large expansion flask of about 5 liters volume was attached to the vacuum line. For convenience we shall describe an experiment with SF_6 although the procedure was the same for C_7F_{14}. After pumping on the entire system for several hours, we isolated the expansion flask, reaction cell, and all gauges except (1). With the main valve to the pumps closed, a few microns of SF_6 were permitted into the system. This was usually done by freezing the SF_6 out with liquid oxygen, opening the SF_6 flask's stopcock and then removing the liquid oxygen bath for a few seconds before closing the stopcock to the SF_6 flask. The pressure of SF_6 was then measured with gauge (1) and stopcock B then closed. The remaining SF_6 could then be pumped away and the stopcocks leading to the reaction cell expansion flask and the other gauges reopened. After a few minutes, the valve leading to the pumps was again closed and stopcock B opened. The new pressure of SF_6 was calculated from a previously determined expansion factor (2.15×10^{-3}). Stopcocks to the expansion flask and gauge (1) were now closed. Then gaseous NO in equilibrium with solid at -196°C was allowed to enter the system by opening the stopcock to its containing flask for about 5 seconds. NO pressure (equilibrium value about .085 torr) was measured with gauge (2), which was then isolated from the main line after a few minutes were allowed for diffusional mixing of SF_6 and NO. Helium was then let into the system until the total pressure was about 18 torr. About 5 minutes more (at least) was allowed for diffusional mixing before experimental

data were taken.

For C_3F_8, C_2F_4 and SiF_4, pressure of these gases were in the micron range and the loading technique was slightly modified. The expansion flask was not required and was kept isolated. After taking the pressure reading with gauge (1), stopcock A was closed and the fluorine-containing substance was trapped out in a cold finger at -183°C. This was thought desirable since the higher pressures used here increased the possibility of contaminating the NO supply during the time NO was let into the system. After the NO pressure had been measured the fluorine-containing substance was allowed to evaporate again. The rest of the procedure followed that given before. Of course, in later work on NO alone, the NO was simply released into the system and its pressure measured with gauge (2).

2.III The Pulsed Lamp

The lamp shown in detail in Fig. 3 consisted of a quartz cell 2.5 cm in diameter with a LiF window sealed on with epoxy cement or silicone resin. Power for creating an electrical discharge in the lamp is supplied to the microwave excitation cavity through S band waveguide from a pulsed magnetron. A pyrex and lucite water jacket helps attenuate stray microwave power from the lamp cavity which would otherwise penetrate the detection cavity and cause undesirable discharge in the reaction cell. Tubular metal ears on both cavities act as waveguide below cutoff and help to prevent microwave power leakage between cavities.

In our early experiments (SF_6, C_7F_{14}), both lamp and reaction cell were sealed to the same LiF window with Armstrong C_7 - W epoxy cement. Kr gas was used in the lamp, usually in the range 10-40 torr in order to reduce the power leakage from the excitation to the detection cavity. The Kr lamp emits its principal ionizing radiation at 1236Å (10.0 eV).

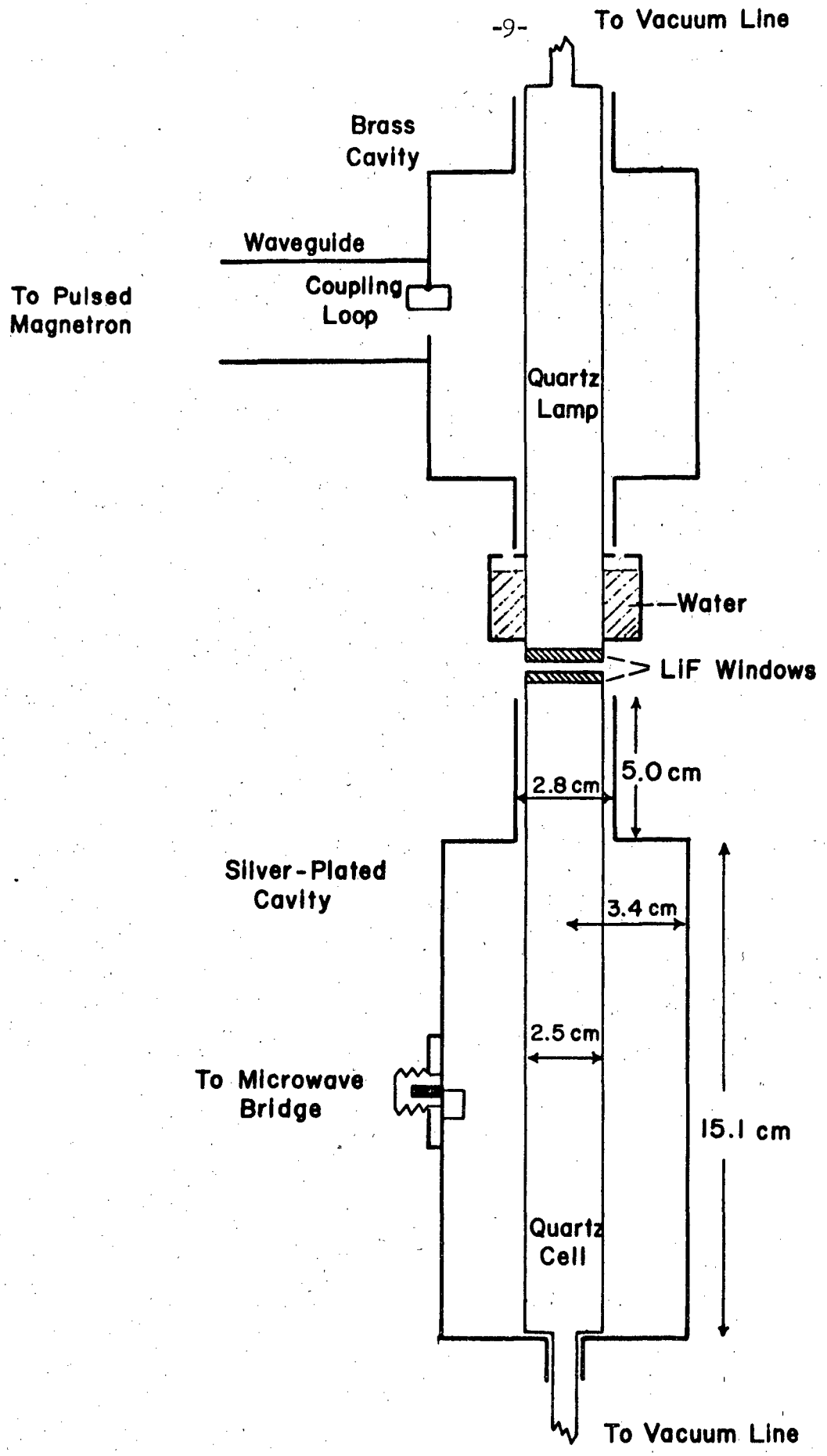

Fig. 3 Lamp and reaction cell

Later it was decided to separate the lamp and the reaction cell by about 2 mm and use hydrogen in the lamp, the pressure being in the range 10-30 torr. The 1216 Å Lyman α line provides the principal radiation for NO ionization and much of the remaining radiation from the lamp is attenuated by atmospheric oxygen bands. Although most of the photons of energy greater than 9.2 eV absorbed in NO produce ionization,[10] it is desirable to reduce the possibility of photodissociating the NO[11] which is energetically possible above 6.5 eV.

The electronic circuit for the pulsed magnetron system is given in Figs. 4 and 5. The pulse forming network is charged to 8 kilovolts and is designed to be fired by a thyratron giving a square voltage pulse lasting 2.5 microseconds. This pulse is transformed to 18 kilovolts and applied to the magnetron which has a peak power rating of 120 kilowatts. The damping diode prevents continued oscillation of the pulsing network after the initial 2.5 microsecond pulse. The duration of the lamp flash with respect to emission of ionizing radiation for NO was experimentally determined as about 40 microseconds by observing the initial rise of electron concentration with just NO and helium in the reaction cell.

2.IV Electron Concentration Measurements

The frequency counting apparatus is shown in the block diagram in Fig. 1. This equipment consisted of a Dymec DY 5796 transfer oscillator, a Hewlett Packard 540 B transfer oscillator and a Hewlett Packard 524 D electronic counter with a 525 B frequency converter. As is shown in Chapter 3, the free electron concentration, n, in the cavity can be related to a shift, Δf, in the cavity resonance frequency, caused by the presence of the electrons. An evaluation of this relation for various experimental conditions has been given by Biondi.[5] For our purposes, it

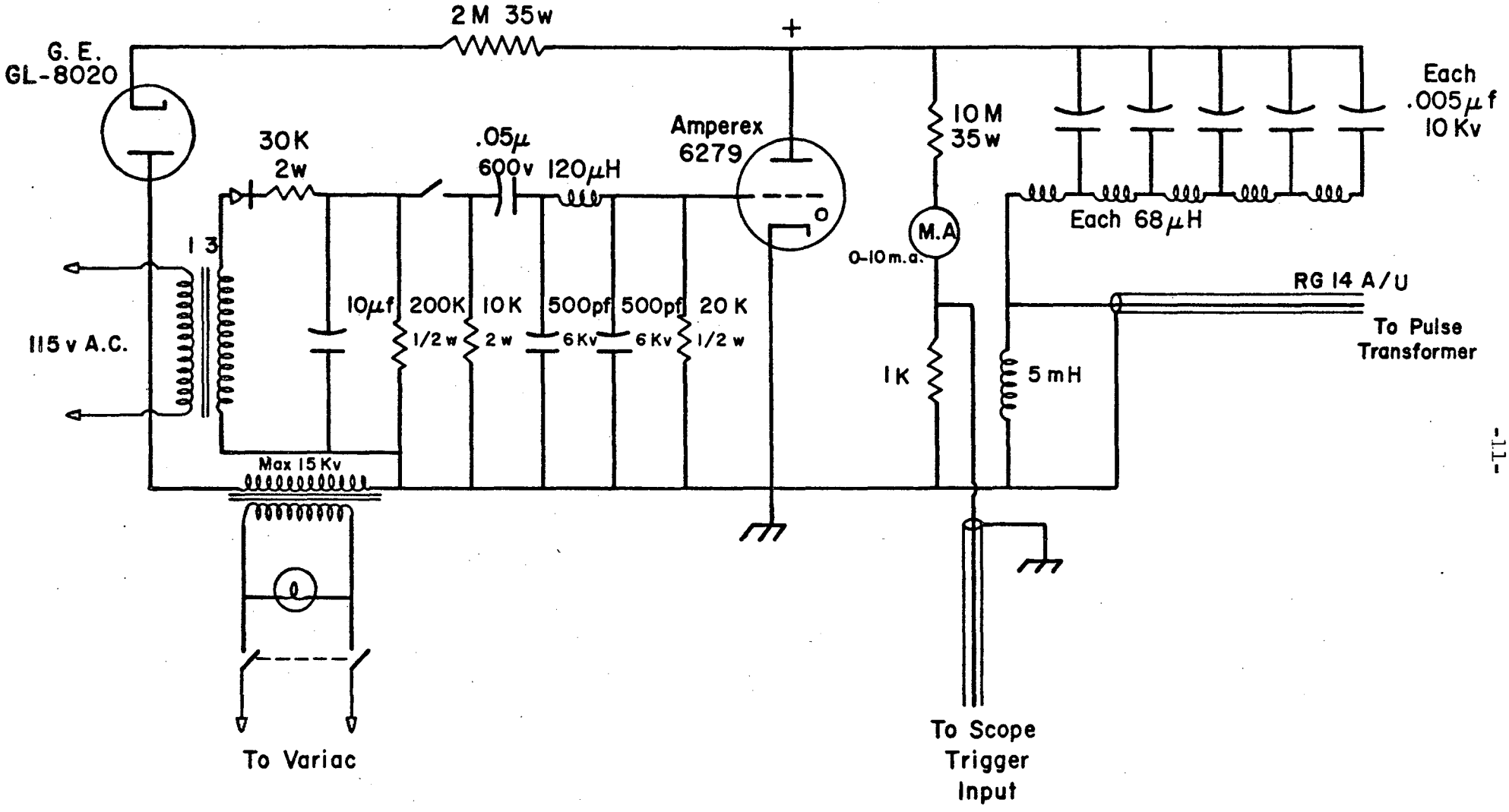

Fig. 4 Pulsed magnetron electronics (1)

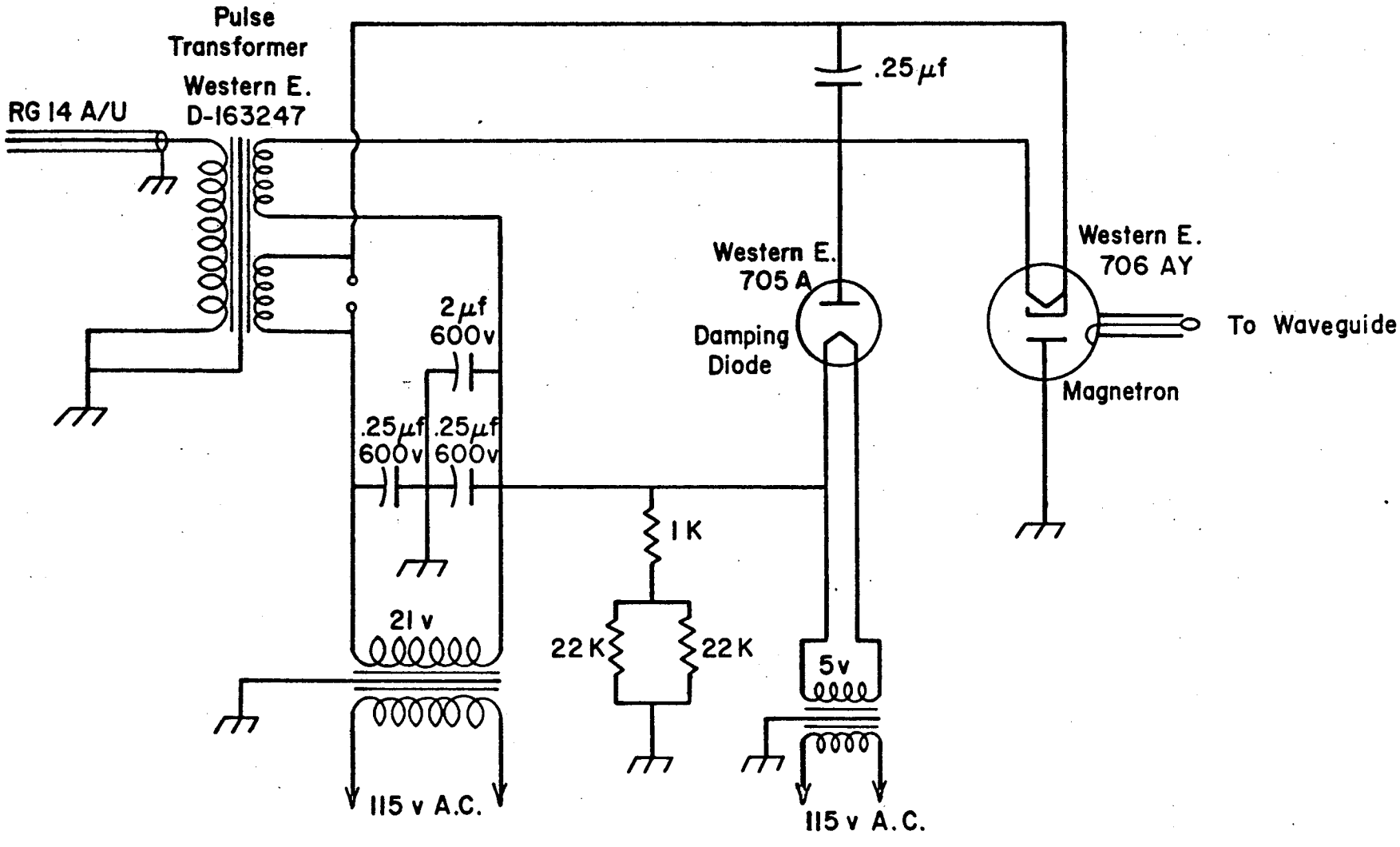

Fig. 5 Pulsed magnetron electronics (2)

is sufficiently accurate to assume that the electrons are uniformly distributed in the reaction cell. This results in the relation

$$n = 6.74\times10^{-8}\ f\ \Delta f \quad \text{electrons/cc} \qquad (2\text{-}1)$$

where n is the (uniform) electron concentration in the reaction cell and f is the cavity resonant frequency ($2\pi f = \omega$) and Δf is the frequency shift. Δf can be determined for experimental data such as in Fig. 6b by relating the displacement of the curve from its $t = \infty$ value to the frequency shift for a corresponding displacement in the A-B portion of Fig. 6a. The absolute electron concentration was not actually needed for the analysis of the electron attachment data (an exponential decay) but was useful for insuring that various restricting conditions were not violated (see Chapter 3).

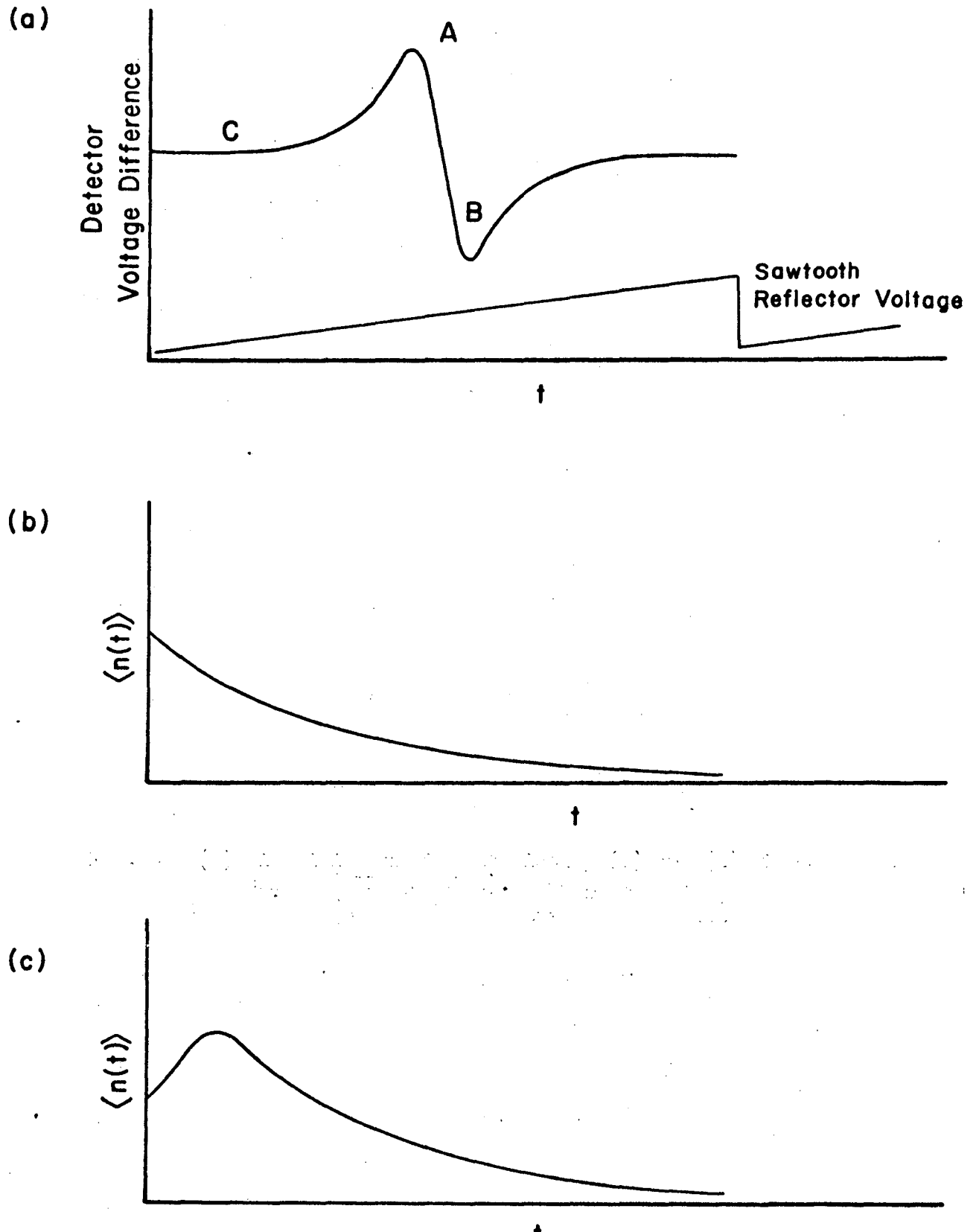

Fig. 6 (a) Discriminator Characteristic; (b) and (c) Electron Decay Curves (illustrative).

3. BASIS OF THE EXPERIMENTAL METHOD

3.I. Conductivity of Ionized Gas

Consider a cloud of gaseous electrons, negative ions, and positive ions with concentrations n_e, n_-, and n_+ particles per cc respectively, satisfying a condition of approximate charge neutrality $n_e + n_- - n_+ \simeq 0$. We refer to such an assembly as a plasma, noting that there may also be various uncharged species present. For electromagnetic methods of determining the electron concentration in the bulk plasma to be effective, the plasma must act as a transparent dielectric to the probing wave. The important parameter, in this connection, is called the plasma frequency $\omega_p = 4\ n_e e^2/m$ cps, where m and e are, respectively, the electronic mass and charge. If the angular frequency of the probing signal, ω, is greater than ω_p, the signal can pass freely through the plasma; if $\omega < \omega_p$, serious reflections occur near the plasma boundary. For the probing frequency employed of about 3150 Mc/sec, the above condition places an upper limit on measurable electron concentrations of about 5×10^{11} electrons per cc. It will be seen later that other considerations reduce this estimate somewhat.

For $\omega > \omega_p$ it is meaningful to define a conductivity $\sigma = \underline{J}/\underline{\epsilon}$ where $\underline{J}$ represents the current density due to free electrons and $\underline{\epsilon} = \underline{E}\epsilon^{i\omega t}$ refers to the electric vector of the applied high frequency field. In general, σ is complex, containing contributions both in phase and quadrature with the applied field.

High frequency conduction and dispersion in plasmas has been extensively investigated theoretically.[6,12-20] Margenau[17] has shown how to derive the relation between the velocity distribution and the complex conductivity under fairly general conditions. One need only assume that the

distribution of electrons in coordinate and velocity space does not change in time over an interval long compared with the microwave period. It is noted that the velocity distribution of the electrons may correspond to a temperature which is not that of the ions and molecules. Also the electron velocity distribution may assume non-Maxwellian forms. If the distribution function, $f(\underline{v})$, is expanded in spherical harmonics keeping only first-order terms, we have

$$f(\underline{v}) = f_o(v) + \gamma\, v_x(f_1(v) - ig_1(v))\epsilon^{i\omega t} \tag{3-1}$$

where $\gamma = eE/m$, e and m being the electronic charge and mass, and E the electric field strength (directed in the x direction). The Boltzmann transfer equation[21]

$$\gamma\epsilon^{i\omega t}\frac{\partial f}{\partial v_x} + \frac{\partial f}{\partial t} = \frac{Df}{Dt} \tag{3-2}$$

provides, after some manipulation, a relation between the isotropic part, f_o, and the nonisotropic parts, f_1 and g_1, of the velocity distribution function. From this is obtained an expression for the conductivity

$$\sigma = \frac{ne\bar{v}_x}{\underline{E}} = -\frac{ne^2}{3m}\int \frac{\nu - i\omega}{\omega^2 + \nu^2}\frac{\partial f_o^o}{\partial v}\, v\, d\underline{v} \tag{3-3}$$

$$= \frac{ne^2}{3m}\int \frac{\partial}{\partial v}\left(\frac{\nu - i\omega}{\omega^2+\nu^2}\, v^3\right) 4\pi f_o^o\, dv \tag{3-4}$$

where f_o^o represents f_o when unperturbed by the electric field, and the normalization condition is $\int 4\pi v^2 f_o^o dv = 1$. The momentum transfer collision frequency[22] for collisions of electrons with molecules and ions is represented by ν. In general, it depends on the types of molecules and ions present and on the electron velocity, v. (In future

equations, when n appears without subscript, it refers to the free electron concentration.) From the mass dependence of Eqs. (3-3) and (3-4), we see that contributions to the conductivity from ions present would be expected to be negligible, compared to the electronic contribution. Equations (3-3) and (3-4) have been derived previously under less general assumptions than here.[6]

Several special cases are useful.

(1) ν not a function of v. This assumption is not very accurate physically, but leads quickly to a formula for σ which is a useful limiting case:

$$\sigma = \frac{ne^2}{m}\left(\frac{\nu - i\omega}{\omega^2+\nu^2}\right) \qquad (3\text{-}5)$$

This is the Lorentz expression, derivable from the simple velocity-damped oscillator equation

$$m\frac{d^2x}{dt^2} + \nu m \frac{dx}{dt} = eE\epsilon^{i\omega t} \quad .$$

The case $\nu \ll \omega$ is a good approximation in many gases at pressures of a few tens of torr, giving the result

$$\sigma = -ine^2/m\omega \qquad (3\text{-}6)$$

(2) Electrons uniformly distributed in energy in the interval $0 < v < v_1$. In this case[17]

$$\sigma = \frac{ne^2}{m}\left(\frac{\nu_1 - i\omega}{\omega^2 + \nu_1^2}\right)$$

which is the same functional form as in the Lorentz formula but refers to the collision frequency ν_1, of the fastest electrons in the distribution.

(3) Electrons form a Maxwellian distribution at arbitrary temperature T. In this case

$$\sigma = \frac{ne^2}{m} \cdot \frac{8}{3\sqrt{\pi}} \left(\int_0^\infty \epsilon^{-u^2} \frac{\nu u^4}{\omega^2+\nu^2} du - i\omega \int_0^\infty \epsilon^{-u^2} \frac{u^4}{\omega^2+\nu^2} du \right) \quad (3\text{-}7)$$

where $u = (m/2k_BT)v$ and k_B is Boltzmann's constant. Expression (3-7) has been evaluated[6] in terms of tabulated functions and the following limiting approximations are useful[23]

$$(\nu^2 \ll \omega^2) \quad \sigma = \frac{ne^2}{m\omega} \left[\frac{4}{3} \cdot \frac{\nu}{\omega} \left(1 - \frac{3\pi}{4} \left(\frac{\nu}{\omega}\right)^2 \right) - i \left(1 - \frac{5\pi}{8} \left(\frac{\nu}{\omega}\right)^2 \right) \right] \quad (3\text{-}8)$$

$$(\nu^2 \gg \omega^2) \quad \sigma = \frac{ne^2}{m\omega} \left[\frac{8}{3\pi} \cdot \frac{\omega}{\nu} \left(1 - \frac{4}{\pi} \left(\frac{\omega}{\nu}\right)^2 \right) - i \left(\frac{8}{3\pi} \right) \left(\frac{\omega}{\nu} \right)^2 \left(1 - \frac{8}{\pi} \left(\frac{\omega}{\nu}\right)^2 \right) \right] \quad (3\text{-}9)$$

An earlier investigation[6] showed that under the weaker assumptions that the electrons can only acquire energy from the external electric field and can only undergo elastic collisions with gas at temperature T, the distribution function f_o is obtained as

$$\ln f_o = -\int_0^{v^2} \frac{\frac{m}{2} d(v^2)}{k_BT + \frac{M\gamma^2\lambda^2}{6(v^2+\omega^2\lambda^2)}} \quad (3\text{-}10)$$

where $\lambda = v/\nu$, $\gamma = eE/m$, and M is the mass of a gas molecule. If the second term in the denominator of Eq. (3-10) is negligible with respect to k_BT, the distribution is clearly Maxwellian. Further, numerical investigation shows that in the entire range $k_BT \geq M\gamma^2/6\omega^2$ the distribution function f_o is closely approximated by a Maxwellian distribution

corresponding to a temperature $T' = T(1 + M\gamma^2/6\omega^2 k_B T)$. In our apparatus, during an electron decay experiment, it is true that the probing field is the only source of energy for the thermalized electrons. Also the approximation of elastic collisions only may be reasonable. We shall use the above criterion later to estimate the maximum desirable field strength in the microwave cavity. We note in passing that for sufficiently large electric field strengths, the distribution function for the electrons

$$f_o = A\epsilon^{-\frac{3m(v^4+2\omega^2\lambda^2v^2)}{2M\gamma^2\lambda^2}}$$

resembles the Druyvesteyn distribution. To obtain f_o from Eq. (3-10), λ was assumed constant.

3.II. The Microwave Cavity

In our experiments, the electron reactions studied take place in a quartz cell which is contained in a cylindrical microwave cavity, as shown in Fig. 3. Maxwell's equations, when solved for the case of a region surrounded by metallic boundaries give rise to eigenvalue equations which determine the set of possible wavelengths and corresponding field configurations in the cavity. Results for many practical cavities have been tabulated.[24] By supplying the microwave energy of frequency corresponding to a particular mode of oscillation in the cavity we can excite that mode preferentially. Because of imperfections in the cavity such as coupling holes to the waveguide, we cannot eliminate interaction between modes, i.e., we cannot suppress undesired modes completely.

For a cylindrical resonator of radius R and height h with completely closed, perfectly conducting walls, the resonant frequencies

and corresponding field configurations are given below.

Transverse Magnetic Modes:

$$E_z(r, \phi, z) = E_o J_m\left(\frac{x_{mn}}{R} r\right) \epsilon^{\pm im\phi} \cos\left(\frac{p\pi z}{h}\right) \qquad (3\text{-}11)$$

$$B_z(r, \phi, z) = 0$$

$$\omega_{mnp} = c\sqrt{(x_{mn}/R)^2 + (p\pi/h)^2} \qquad p = 0, 1, 2, \ldots$$
$$m = 0, 1, 2, \ldots$$
$$n = 1, 2, 3, \ldots$$

where J_m is the Bessel function of order m, x_{mn} is the nth root of $J_m(x) = 0$, and $c = 3\times10^{10}$ cm/sec.

Transverse Electric Modes:

$$B_z(r, \phi, z) = E_o J_m\left(\frac{x'_{mn}}{R} r\right) \epsilon^{\pm im\phi} \sin\left(\frac{p\pi z}{h}\right) \qquad (3\text{-}12)$$

$$E_z(r, \phi, z) = 0$$

$$\omega_{mnp} = c\sqrt{(x'_{mn}/R)^2 + (p\pi/h)^2} \qquad p = 1, 2, 3, \ldots$$
$$m = 0, 1, 2, \ldots$$
$$n = 1, 2, 3, \ldots$$

where x'_{mn} is the nth root of $J'_m(x) = 0$, $c = 3\times10^{10}$ cm/sec.

In the above, the axis of the cavity is taken to be along the z axis. The actual cavity used has walls of finite conductivity containing various holes all of which tend to shift the observed resonant frequencies from the values which can be calculated from the above formulas. The field configurations are likewise perturbed. In a case where actual measurements were carried out, using probe techniques, on a cavity similar in shape

to ours, the fields were found to conform closely to the ideal values, except very near the upper orifice.[25]

As shown in Eq. (3-18), the measured electron concentration is actually an average over the spatial electric field distribution in the cavity. For this reason it is desirable to have the electric field relatively uniform in the region of the cavity containing the free electrons, i.e., close to the axis of the cavity. The TM_{010} mode of a cylindrical cavity proves to be convenient for this purpose, the E field being parallel to the cavity axis with spatial distribution given by

$$E_z(r) = EJ_o\left(\frac{x_{o1}}{R}\, r\right) \qquad (3\text{-}13)$$

independent of z or ϕ. Calculations with Eqs. (3-11) and (3-12) show that for the dimensions of our cavity the supplied frequency of 3150 Mc/sec is consistent with the excitation of the TM_{010} mode, to the exclusion of all other TM and TE modes except possibly TM_{01p} modes with p = 1,2,... . Experiments involving the insertion of dielectric material into the resonating cavity seemed to eliminate the possibility of many axial nodes in E_z. Since axial variation of electron concentration in the cell should be small, averaging over the fields for TM_{010} and TM_{011} modes, for example, should give nearly the same answer. Hence, for calculation of field-averaged electron concentrations, it was assumed that the TM_{010} mode was exclusively excited.

Near a particular resonant frequency, ω_o, of the cavity, it is a good approximation to write the cavity impedance as the sum of a term Z_1, slowly varying with frequency plus a term exhibiting resonance[26]

$$Z = Z_1 + \frac{1/Q_{ext}}{i\left(\frac{\omega}{\omega_o} - \frac{\omega_o}{\omega}\right) + \frac{1}{Q} + \frac{1}{\epsilon_o \omega_o} \cdot \frac{\int \underline{J} \cdot \underline{E}\, dV}{\int \underline{E} \cdot \underline{E}\, dV}} \qquad (3\text{-}14)$$

where ω_o and Q are the resonant frequency and Q of the cavity when no perturbing current density $\underline{J}$ is present. ϵ_o is the permitivity of free space and the integration is over the enclosed volume of the cavity. Q_{ext} refers to losses external to the cavity and is related to Q through a coupling parameter β by

$$Q_{ext} = Q/\beta.$$

The final term in the denominator of Eq. (3-14) results from the presence of free electrons in the cavity. As these electrons disappear, they produce a time-dependent shift $\Delta\omega$ in the resonant frequency of the cavity plus a time-dependent change in the loss 1/Q expressed by[26]

$$\Delta(1/Q) - 2i\Delta\omega/\omega_o = \frac{1}{\epsilon_o \omega_o} \frac{\int \underline{J} \cdot \underline{E}\, dV}{\int \underline{E} \cdot \underline{E}\, dV} \qquad (3\text{-}15)$$

Splitting the conductivity σ into its real and imaginary parts ($\sigma = \sigma_r + i\sigma_i$), we derive from Eq. (3-15)

$$2\frac{\Delta\omega}{\omega_o} = -\frac{1}{\epsilon_o \omega_o} \frac{\int \sigma_i E^2\, dV}{\int E^2\, dV} \qquad (3\text{-}16)$$

and

$$\Delta\left(\frac{1}{Q}\right) = \frac{1}{\epsilon_o \omega_o} \frac{\int \sigma_r E^2\, dV}{\int E^2\, dV} \qquad (3\text{-}17)$$

Using the expression for σ from Eq. (3-5), noting that $\omega \simeq \omega_o$, we obtain from Eq. (3-16)

$$\frac{\Delta\omega}{\omega_o} = \frac{e^2}{2m\epsilon_o\omega_o^2} \cdot \frac{1}{1+(\nu/\omega)^2} \frac{\int n(\underline{r},t)E^2(\underline{r})dV}{\int E^2(\underline{r})\, dV} \qquad (3\text{-}18)$$

where the dependence of n on spatial and time variables has been emphasized. We see that direct measurement of $(\Delta\omega/\omega_o)$ as a function of time can yield the time variation of electron concentration averaged over the electric field in the cavity which we shall call $\langle n \rangle$. A method employing this approach has been given by Biondi.[5] Essentially, one point on a $\Delta\omega$ vs. time curve is obtained for each electron decay experiment by observing the time at which the power absorbed by the cavity increases sharply, indicating passage through resonance. This time is varied by shifting the probing frequency slightly from experiment to experiment thus obtaining a complete $\Delta\omega$ vs. time curve. This method has drawbacks for experiments on systems whose chemical composition may change as the result of the photoionization or electron decay processes since the electron decay curve obtained would not be characteristic of the gas initially present.

The microwave apparatus employed in our research, shown schematically in Fig. 1, was designed to permit a continuous record of electron concentration as a function of time during a single electron decay experiment. A PRD Electronics type 815 klystron power supply was employed for supplying the cathode and reflector voltages to a Raytheon RK707B reflex klystron which was adjusted to operate at about 3150 Mc/sec in a frequency band containing the cavity resonant frequency. A special D.C. power supply was constructed for supplying heater current since it was found that objectionable 60 cps variation of the output frequency could thus be considerably suppressed. The directional isolator reduces the

influence of the rest of the microwave circuit on the klystron output frequency. A small amount of power is bled off for the purpose of frequency determination and the rest is passed through a 0 to -20 db attenuator to the Pound[27] discriminator circuit. Essential to this circuit is a "magic T"[24] with its collinear arms terminated in the resonant cavity and an adjustable tuning short and microwave detectors mounted on the other two arms. The signal from the detectors is sent into a type D differential amplifier of a type 545 Tektronix oscilloscope. In the "magic T", the incoming probing wave splits equally between the collinear arms resulting in waves of the same phase. If the collinear arms were terminated in identical impedances, no microwave energy could reach the detector on the vertical arm, whereas if one of the impedances introduced a 180° phase shift, all the reflected energy would reach the vertical detector. In practice, the tuning short is adjusted so that the detectors each see the same signal strength when the signal frequency is held exactly at the resonant frequency of the cavity or far away from that frequency. If the klystron frequency is increased linearly with time by adding a small sawtooth contribution to the reflector voltage, a typical discriminator pattern, shown in Fig. 6a, can be obtained on the oscilloscope. It should be noted that near the resonant frequency, reflector voltage change and klystron frequency change are proportional. The region of linear variation between points A and B is of special interest to us. In performing an electron decay experiment, one fixes the klystron reflector voltage at a position corresponding to point B on the discriminator curve. When free electrons are produced in the cell by photoionization the resonant frequency of the cavity is shifted. Alternatively, we can say that there is a large contribution to the

imaginary part of the denominator in expression (3-14) giving rise to a shift in the phase of the cavity impedance. The effect on the signal reaching the detectors closely reproduces the situation where the klystron frequency is swept. A typical single sweep trace on the oscilloscope starting the instant that the lamp is fired is shown in Fig. 6b. The initial rapid rise of electron concentration following the firing of the lamp takes place in about 40 μsec and is barely observable on the time scales usually employed to observe electron decay. For initial concentrations of 10^7 to 10^8 electrons per cc used in our experiments, the oscilloscope trace showed deflections within the linear region A-B. In some preliminary investigation, larger initial electron concentrations were produced, resulting in deflections corresponding to the portion C-B of the discriminator curve. This resulted in oscilloscope traces similar to that shown in Fig. 6c, where the rising and then falling curve corresponds to monotonic decrease in electron concentration. Such large electron concentrations were not employed during quantitative measurements on electron attachment rates.

3.III. Range of Applicability

In expression (3-14) it is assumed that the term representing electron current represents a small perturbation of the cavity. This is equivalent to the condition $|\sigma| \ll \omega\epsilon_o$. As a useful approximation, consider the case where the frequency, ν, of electron collisions with the gas present is much smaller than the angular frequency, ω, of the E field (a condition satisfied for most of the experiments performed). We then obtain the requirement

$$n \ll m\omega^2\epsilon_o/e^2 = 3.2\times10^{-10}\ \omega^2 \text{ electrons/cc.}$$

This condition requires electron concentrations much less than 10^{11} per cc at the employed frequency.

A detailed consideration of further limiting factors has been made by Persson.[28] For the case $\nu/\omega \ll 1$, the upper limit on electron density is determined by the electric polarization of the plasma, which corresponds to "plasma resonance" mentioned in Section 3.I. For an error of less than 5% in the measurement of electron concentration at 3000 Mc/sec, the permissible maximum value is about 6×10^{9} per cc. The lower limit for measureable electron concentrations is determined only by the minimum cavity perturbation which can be observed. In our case, the limiting factor was a small 60 cps fluctuation of the klystron frequency about its steady value, caused by small residual ripples on its various D.C. voltages. However, initial concentrations of 10^{7} electrons per cc could be comfortably observed over a factor of 10 decrease.

When ν becomes comparable with ω, or larger, one must consider the effect of the plasma in exciting higher modes in the cavity. It is hard to get a quantitative estimate of this effect but for the most extreme case considered by Persson,[28] the maximum electron concentration is placed at about 2×10^{8} electrons per cc. Higher electron concentrations than this were not employed in our experiments.

From the expression derived following Eq. (3-10), we can obtain a limit for the maximum power which can be used in the probing signal consistent with the electron temperature being close to that of the gas, i.e., about 300°K. Following the procedure suggested by Oskam,[23] we denote by P_o the power fed into the cavity at resonance and by definition of Q

$$P_o = \frac{1}{2} \epsilon_o \frac{\int E^2 \, dV}{Q/\omega_o} \qquad (3\text{-}19)$$

where the integration is over the cavity volume. Equation (3-19) converts the inequality for the field $E^2 \ll 6m^2 \omega^2 k_B T/Me^2$ to a condition on the power

$$P_o \ll 3m^2 \omega_o^3 \epsilon_o k_B T \int J_o^2 \left(\frac{x_{01}}{R} r\right) dV/Me^2 Q$$

where E has been taken to be its maximum value in the cavity for the TM_{010} mode and T is the gas temperature. In our case this reduces to

$$P_o \ll 510/A \quad \mu \text{ watts} \qquad (3\text{-}20)$$

where A is the molecular weight of the gas. In deriving this, Q was taken to be the loaded Q of the cavity evaluated as ~5000 from direct bandwidth measurement. Measurements on the apparatus with a bolometer mount replacing the connector to the cavity showed that the maximum power reaching the cavity was 0.32 m.w. with the variable attenuator at 0 db. During attachment experiments, there is further attenuation of -15 db putting the maximum value of P_o at about 10 μw. At this setting, the electron temperature should be close to the gas temperature, at least for experiments in He and Ne. The above analysis is admittedly rough since such effects as coupling to the cavity and electron collisions have been neglected. In general, the experimental data showed little dependence on power-level increase by a factor of 30.

As mentioned before, most of the experiments in this research were carried out at low enough pressures so that the electron collision frequency is small compared with the microwave angular frequency. A simple discussion shows why this is desirable. For convenience in this discussion, we evaluate expressions (3-16) and (3-17) using the simplified

expression (3-5) obtaining

$$(\Delta\omega/\omega_o) = \frac{\langle n(t)\rangle e^2}{2m\,\epsilon_o\,\omega_o^2} \cdot \frac{1}{1 + (\nu/\omega)^2} \qquad (3\text{-}18)$$

and

$$\Delta(1/Q) = \frac{\langle n(t)\rangle e^2}{m\,\epsilon_o\,\omega_o^2} \cdot \frac{(\nu/\omega)^2}{1 + (\nu/\omega)^2} \qquad (3\text{-}21)$$

Expressions (3-18) and (3-21) contribute the imaginary and real increments, respectively, in the denominator of the resonant impedance expression (3-14). Since only the slope of a plot of ln $\langle n(t)\rangle$ against t is required for obtaining the electron attachment rates, the factor $1/[1 + (\nu/\omega)^2]$ which remains constant in time should not be expected to influence the results. However, for $(\nu/\omega)^2 \gg 1$, the perturbing effect of free electrons in the cavity is reduced by the factor $1/[1 + (\nu/\omega)^2]$ so that eventually the difference signal from the detectors becomes lost in background noise. This effect was observed experimentally for Kr and Xe, where $(\nu/\omega)^2$ is large in the pressure region used. Also, we must consider energy losses in the cavity when ν becomes comparable with ω. Expression (3-21) has a maximum at $\nu = \omega$, at which point $(1/Q) = 2\Delta\omega/\omega_o$. Experimentally, $\Delta\omega/\omega_o$ is about 5×10^{-5}, i.e., about 25% of the value of 1/Q. Consideration of Eq. (3-14) indicates that a non-negligible $\Delta(1/Q)$ should introduce an apparent decrease in the phase shift, this error decreasing with $\langle n\rangle$. This would give a curvature to the data on a logarithmic plot such as shown in Fig. 7a. In fact, a slight curvature was observed but it occurred at late times (Fig. 7b) and did not vary from gas to gas. This curvature is attributed to another cause (see Chapter 4).

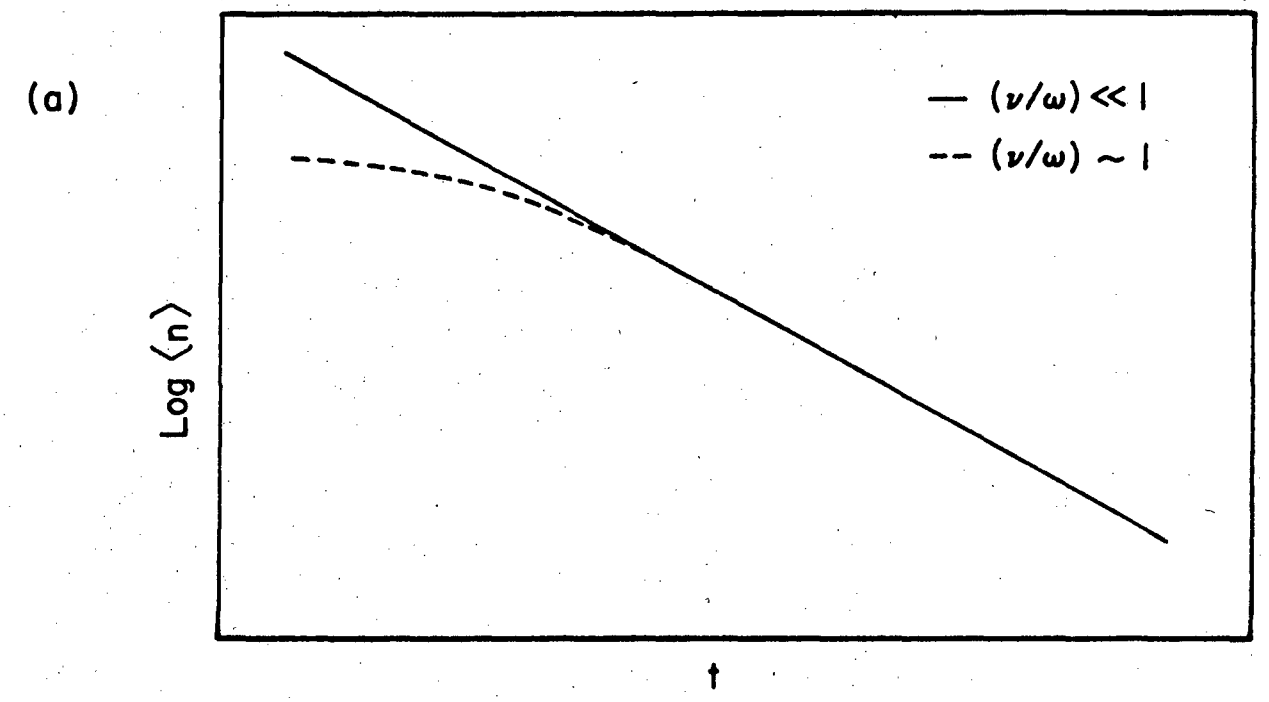

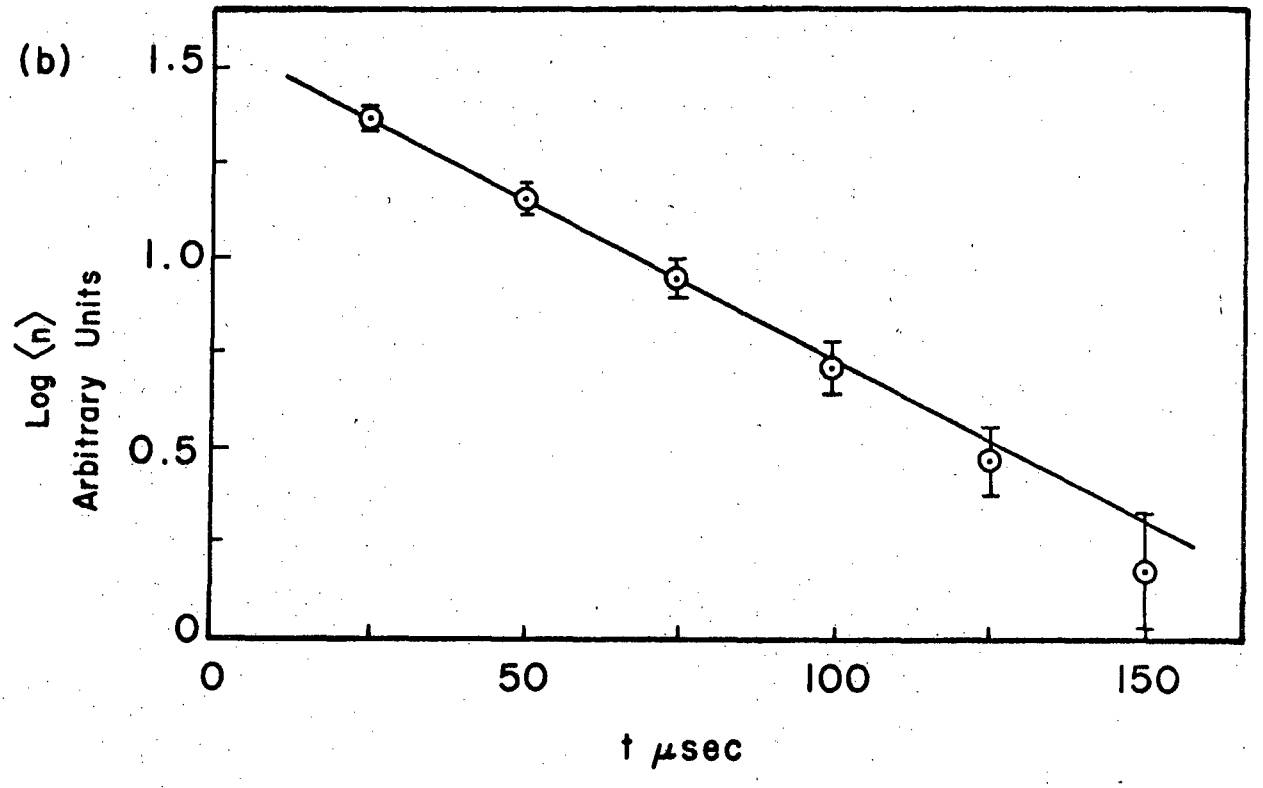

Fig. 7 Electron Decay Curves (a) Illustrative (b) Typical Data for C_7F_{14}.

Table 1 contains the parameter $R = \sigma_i(p)/\sigma_i(0)$, where σ is written as a function of the gas pressure p which is proportional to ν. For $\sigma_i(0)$ we use $-ne^2/m\omega$. In obtaining Table I expressions (3-8) and (3-9) were employed, except for $10 > (\nu/\omega)^2 > 1/10$, when the exact expression (3-7) was used. Values of ν as a function of p were obtained from a published study of collision probabilities by a microwave method.[29] Table 1 gives an estimate of the pressure at which substantial reduction of signal can be expected. It was qualitatively in agreement with experiment.

Table 1. Pressure dependence of $\sigma_i(p)/\sigma_i(0)$ for Maxwellian distribution

Gas	Pressure (torr)			
	100	50	20	10
He	.40	.79	.90	.98
Ne	.93	.98	1.00	1.00
Ar	.97	.99	1.00	1.00
Kr	.06	.22	.66	.81
Xe	.008	.028	.15	.41
N_2	.54	.88	.94	.99

4. FACTORS INFLUENCING THE ELECTRON DECAY RATE

4.I Thermal Equilibrium

All the processes involving the decay of gaseous electron concentration are dependent on the electron energy. In this section, we show that the electrons can be expected to come to thermal equilibrium with the surrounding gas molecules in a very short time compared with the time constant for electron decay. For electrons produced through the photoionization of NO by the 1216 Å Lyman α line, the maximum initial kinetic energy is about 0.9 eV. This is large compared to the average energy of thermal motion at 300°K which is .039 eV. In elastic collisions between fast electrons of kinetic energy u and mass m and gas molecules with thermal kinetic energy and mass M, the average fractional decrease in the electron energy should be close to 2m/M since $m \ll M$. Denoting thermal energy by u_T, we have

$$-\frac{du}{dt} = (2\ m/M)\ (u - u_T)\ \ v/\lambda \qquad (4\text{-}1)$$

where electrons of energy u have velocity v and their mean free path in the gas is λ. Following a calculation by Oskam,[23] we consider the case where the mean free path is independent of electron velocity. Equation (4-1) becomes

$$-\frac{dv}{dt} = (m/M\lambda)\ (v^2 - v_T^2) \qquad (4\text{-}2)$$

where $v_T^2 = (2/m)\ u_T$. The solution to (4-2) is

$$v(t) = v_T\ \frac{e^{gt} + C}{e^{gt} - C} \qquad (4\text{-}3)$$

where $C = \dfrac{v_o - v_T}{v_o + v_T}$ and $g = (2m/M)\ v_T/\lambda$, v_o being the velocity at $t = 0$.

If we wish to know how much time is required for u to come within 10% of u_T (i.e., for v to come within about 5% of v_T) we obtain the requirement

$$t > 3.72 \frac{M\lambda}{2 m v_T} \qquad (4\text{-}4)$$

where we have used the fact that $C \simeq 1$. With l_o the mean free path at a pressure of 1 torr, p the actual gas pressure and A the molecular weight of the gas, we obtain

$$t > 2.94 \times 10^{-4} A (l_o/p) \qquad (4\text{-}5)$$

Using microwave data on thermal electron collisions[29] we obtain, for example

Helium: $l_o = .053$, $t > (62/p) \times 10^{-6}$ sec

Neon : $l_o = .303$, $t > (1800/p) \times 10^{-6}$ sec

Xenon : $l_o = .555 \times 10^{-2}$, $t > (214/p) \times 10^{-6}$ sec

In obtaining the above estimates, we have ignored the possibility of inelastic collisions with molecules present. Electrons with 0.9 eV energy can excite the v = 3 and lower vibration levels in NO as well as many rotational levels. Drift velocity measurements give an estimate of the average fractional energy loss, δ, due to collisions of electrons of mean energy $\bar{\epsilon}$ with gas molecules.[30] Data from ref. 30 for electrons in NO is given below.

$\bar{\epsilon}$ (eV)	$\delta \times 10^4$
.2	110
.4	390
.6	450
.8	380
1.0	320

It is interesting to consider the ratio of the fractional excess energy loss due to elastic collisions with He at 20 torr with the corresponding loss due to inelastic collisions with NO at 85 microns. For $\bar{\epsilon}$ = .4 eV, this ratio is

$$\frac{20(2\ m/M)}{.085\ \delta} = \frac{(20)\ (2.74 \times 10^{-4})}{(.085)(390 \times 10^{-4})} = 1.65$$

Furthermore, collisions with the principal attaching gas, when other than NO, will contribute to the thermalizing of fast electrons in addition to producing direct attachment. We conclude that actual thermalizing times may be somewhat shorter than predicted by (4-5).

All attachment studies with fluorine-containing molecules were carried out with about 18 torr of helium present to reduce diffusion loss of electrons. Even in the worst case (SF_6 at highest pressures studied), Eq. (4-5) predicts thermalizing times of less than 20% of the electron decay time constant. For experiments in NO alone the much slower attachment rate meant that thermalizing times were neglibile.

Equation (4-1) can also be solved easily if it is assumed that the electron collision frequency is independent of the electron velocity. This assumption seems less reasonable than assuming constant mean free path and for helium gives an estimate of the thermalizing time about 2.5 times that predicted by Eq. (4-2).[23]

4.II Rate Processes

Free electrons, in the presence of gaseous molecules and ions can disappear by diffusion to the walls and subsequent neutralization there, by attachment to neutral molecules to form negative ions and by direct neutralization of positive ions. These processes correspond, respectively, to the first, second and third terms on the right hand side of the

following equation

$$\frac{\partial n_e}{\partial t} = - \nabla \cdot \underline{\Gamma}_e - k n_e - \alpha n_+ n_e \qquad (4\text{-}6)$$

In Eq. (4-6) and subsequent equations, we refer to electrons, negative ions and positive ions with subscripts e, -, and + respectively. We represent the density of electron current to the walls by $\underline{\Gamma}$ and particle densities by n. k and α are, respectively, the attachment rate coefficient and the recombination coefficient. In general, these will both depend on the chemical composition of the neutrals and ions present and the energy distributions of all types of particles present. We shall assume, in this discussion, that the energy distribution is Maxwellian at 300°K. Since the number of positive ions produced is equal to the number of free electrons, α is a second order rate coefficient for electron disappearance. The term involving α in Eq. (4-6) proved to be negligible in our experiments. Taking our initial electron density as less than 10^8 per cc and setting α near the upper limit of known electron-ion recombination coefficients (10^{-6} to 10^{-7} cc/sec), we obtain an estimate of the maximum possible rate of decrease of electron concentration due to recombination. We conclude that electron ion recombination could be an electron removal process comparable with attachment only for the smallest attachment cross sections we studied, such as for attachment to NO itself. Even in the case of NO, there was no experimental evidence that electron-ion recombination was important. Plots of log $\langle n_e \rangle$ vs time showed a slight downward curvature such as shown in Fig. 7b whereas a contribution from recombination would produce curvature in the opposite direction over the entire range of t. We therefore drop the third term on the right in further discussion of Eq. (4-6).

Above a minimum density, usually taken to be 10^7 to 10^8 particles per cc,[31] we must consider macroscopic space charge effects in discussing the diffusion of charged species. Free diffusion coefficients are about three orders of magnitude larger for electrons than for positive ions. This means that starting from initial charge neutrality ($n_+ = n_e$) a condition will quickly be reached in which there is a net positive charge throughout most of the diffusion region, except near the walls where there is a narrow sheath containing an excess of electrons. The macroscopic deviations from charge neutrality give rise to electric fields which act on the charged particles. If the particles are given electrostatic energies comparable to their mean thermal kinetic energies, free diffusion can no longer take place. Instead, the electrostatic force produced by the net negative charge in the sheath and the net positive charge elsewhere in the gas retards the motion of the electron to the walls and accelerates the diffusion of the positive ions.

It is helpful to make a brief calculation in one dimension comparing thermal and electrostatic energies. Consider a region in which there are only electrons of density n_e per cc. If the electric field is parallel to the x-axis, Poisson's equation for the electrostatic potential, V, is

$$\frac{d^2V}{dx^2} = -4\pi n_e e$$

where e is the charge on the electron. If we take the electric field to be zero at x = 0, then the electrostatic energy, W, of an electron at x is

$$W = -2\pi n_e e^2 x^2$$

Equating the magnitude of W with the mean energy of thermal motion in one dimension, we have

$$2\pi\, n_e e^2\, x^2 = 1/2\, k_B T \qquad (4\text{-}7)$$

where T is the temperature in °K and k_B is Boltzmann's constant. The distance obtained by solving Eq. (4-7) for x is called the Debye length λ_D, given by

$$\lambda_D = \left(\frac{kT}{4\pi\, n_e e^2} \right)^{1/2} = 6.91 \left(\frac{T}{n_e} \right)^{1/2} \text{ cm.} \qquad (4\text{-}8)$$

If this model is applied to the electron sheath, it is apparent that the thickness of the sheath could not be much greater than λ_D since the electrostatic force tending to disperse the cloud of excess electrons would be large enough to repel electrons diffusing to the sheath at thermal energies. At 300°K, with $n_e = 10^8$ electrons per cc, $\lambda_D = 1.2 \times 10^{-2}$ cm, which is small with respect to the dimensions of the diffusion region.

Consider again the situation where initially $n_+ = n_e$. If the initial charge density is large enough, a steady state will quickly be reached in which a strong enough space charge field is established to equalize the rates of diffusion for electrons and positive ions. Provided the fraction of electrons lost in establishing the steady state is small ($(n_+ - n_e)/ n_+ \simeq 0$) the diffusion process can be described by simple formulae given in the next section ("ambipolar diffusion"). At the other extreme, for a sufficiently small initial charge concentration, essentially all the electrons can be lost to the walls without leaving behind a large enough positive space charge to produce a significant

retarding field ("free diffusion"). At intermediate concentrations, a steady state may be reached but only after a period of free diffusion which has considerably depleted the electron concentration ($(n_+ - n_e)/n_+ \simeq 1$). Such a case should show an initially rapid rate of electron diffusion gradually decreasing to an ultimately steady rate. A short numerical investigation of the dependence of the electron diffusion rate on initial concentration is described in Section 4.IV.

4.III Ambipolar Diffusion

Consider the case where electrons and a single species of positive ion are diffusing to the walls of a vessel containing the charged particles as well as some neutral gas. We assume that a steady state has been reached, in which there is a net positive charge in the gas, giving rise to an electric field, $\underline{E}(\underline{r})$ which is large enough to prevent free diffusion but small enough so that the concept of mobility is meaningful. Mobility is the ratio of the drift velocity of a charged particle to the local electric field and is represented by the symbol K. Under the above conditions, the charged particle concentrations will decrease with time according to Eqs. (4-9) and (4-10)

$$\frac{\partial n_e}{\partial t} = -\nabla \cdot \underline{\Gamma}_e$$
$$\frac{\partial n_+}{\partial t} = -\nabla \cdot \underline{\Gamma}_\pm \qquad (4\text{-}9)$$

where

$$\underline{\Gamma}_e = -D_e \nabla n_e - K_e \underline{E} n_e = D_{ae} \nabla n_e$$
$$\Gamma_\pm = -D_+ \nabla n_+ + K_+ \underline{E} n_+ = D_{a+} \nabla n_+ \qquad (4\text{-}10)$$

D_e, D_+ and D_- are constants for free diffusion. Equation (4-10) may be taken as a definition of ambipolar diffusion constants D_{ae} and D_{a+}. (Other symbols in (4-9) and (4-10) have the same meaning as in Section 4.II.) The assumption that quasi neutrality is preserved in time gives

$$\frac{\partial}{\partial t} (n_+ - n_e) = - \nabla \cdot (\underline{\Gamma_+} - \underline{\Gamma_e}) \simeq 0$$

From this, we realize that we can put $\underline{\Gamma_+} \simeq \underline{\Gamma_e} \simeq \underline{\Gamma}$, say, and similarly $n_+ = n_e = n$ and $D_{a+} = D_{ae} = D_a$. From Eq. (4-10) we get

$$\underline{E} = -\left(\frac{D_e - D_+}{K_e + K_+}\right) \cdot \frac{\nabla n}{n} \simeq - \frac{D_e}{K_e} \cdot \frac{\nabla n}{n} \qquad (4\text{-}11)$$

where we have used the fact that $D_e >> D_+$ and $K_e >> K_+$. Also, we have

$$D_a = \frac{K_e D_+ + K_+ D_e}{K_e + K_+} \qquad (4\text{-}12)$$

Using the Einstein relation between diffusion and mobility $K/D = e/k_B T$ where the particles with electronic charge e have temperature T, (k_B being Boltzmann's constant) we have for the case of an isothermal plasma (Section 4.I) $D_a \simeq 2 D_+$. The real advantage in using amibpolar diffusion coefficients is that the system of Eqs. (4-9) and (4-10) reduces to

$$\frac{\partial n}{\partial t} = D_a \nabla^2 n \qquad (4\text{-}13)$$

which describes the behaviour of either electrons or positive ions. The solution to Eq. (4-13) can be given in the standard form

$$n(\underline{r},t) = \sum_{i=1}^{\infty} c_i X_i(\underline{r}) \, e^{-t/\tau_i} \qquad (4\text{-}14)$$

where c_i are constants and X_i are eigenfunctions for the region in which diffusion takes place, satisfying

$$(\nabla^2 + 1/\Lambda_i^2)\ X_i = 0 \qquad (4\text{-}15)$$

The Λ_i, known as the characteristic diffusion lengths, are eigenvalues corresponding to the eigenfunctions X_i and are completely determined by the dimensions of the region in which Eq. (4-15) is solved. The τ_i in Eq. (4-14) are given by $D_a\tau_i = \Lambda_i^2$.

A sufficiently good approximation to our experimental situation is to consider the electrons to be contained in an infinite cylinder of radius a. Then

$$X_i(r) = J_o\left((x_{oi}/a)\ r\right) \qquad (4\text{-}16)$$

and

$$\tau_i = (a/x_{oi})^2/D_a$$

where r is the radial co-ordinate, J_o is the Bessel function of order zero and x_{oi} is the ith root of $J_o(x) = 0$. It is often convenient to consider the case of diffusion in the fundamental mode [only the i = 1 term present in Eq. (4-14)] since this is a simple exponential decay. We note that the higher modes decay rapidly with respect to the fundamental mode for example

$$\frac{\tau_2}{\tau_1} = \left(\frac{2.40}{5.52}\right)^2$$

and

$$\frac{\tau_3}{\tau_1} = \left(\frac{2.40}{8.65}\right)^2$$

for the infinite cylinder. In this case, when $t = \tau_1/2$, the contribution of the second diffusion mode, relative to the fundamental mode, has decreased to 13% of its initial value. In addition to this, the contribution of higher modes may be quite small even at t = 0, since the

initial electron concentration is distributed in proportion to the intensity of photoionizing radiation, which should be greatest at r = 0, falling off as r → a.

It can be shown[23,7] that, in the case where electrons, positive ions, and negative ions are present, the diffusion problem can be handled in a manner analogous to the ambipolar treatment of the Eqs. (4-9) and (4-10). In the present case, the diffusion equations are

$$\frac{\partial n_e}{\partial t} = D_{ae} \nabla^2 n_e$$

$$\frac{\partial n_+}{\partial t} = D_{a+} \nabla^2 n_+ \qquad (4\text{-}17)$$

$$\frac{\partial n_-}{\partial t} = D_{a-} \nabla^2 n_-$$

where we must now employ separate ambipolar diffusion constants for the different species. In this connection, we require the parameter $\beta = n_-/n_e$. Provided[7] $\beta < 100$ we have, in the isothermal case

$$D_{ae} \simeq 2(1 + \beta)D_+$$

$$D_{a+} \simeq 2D_+ \qquad (4\text{-}18)$$

$$D_{a-} \simeq 2(1 + \beta)(D_+/D_e)D_-$$

and

$$\underline{E} \simeq - \frac{D_e}{K_e} \cdot \frac{\nabla n_e}{n_e}$$

We note that, in the present approximation, neither the space charge field nor the diffusion of positive ions is altered when negative ions are present.

Finally we mention that Biondi[7] has also considered the solution of Eq. (4-17) in the case where attachment to form negative ions takes place simultaneously with diffusion. The appropriate equations are

$$\frac{\partial n_e}{\partial t} = D_{ae} \nabla^2 n_e - k n_e$$

$$\frac{\partial n_+}{\partial t} = D_{a+} \nabla^2 n_+ \qquad (4\text{-}19)$$

$$\frac{\partial n_-}{\partial t} = D_{a-} \nabla^2 n_- + k n_e$$

with D_{ae}, D_{a+} and D_{a-} given by Eq. (4-18). If we make the plausible assumptions that

(i) for positive ions diffusion is entirely in the fundamental mode

$$n_+(t) = n_+(0)\, e^{-t/\tau} \qquad \text{where } D_{a+}\tau = \Lambda_1^2$$

(ii) $D_{a-} \nabla^2 n_- \ll k n_e$

we can easily obtain from the quasi-neutrality condition,

$$\frac{\partial}{\partial t} (n_e + n_- - n_+) \simeq 0,$$

the equation

$$\frac{\partial n_e}{\partial t} = - k n_e - n_+(t)/\tau \qquad (4\text{-}20)$$

If Eq. (4-20) is integrated subject to the condition $n_+(0) = n_e(0)$, we obtain

$$n_e(t) = \frac{n_e(0)}{1 - 1/k\tau} \left(\epsilon^{-kt} - \frac{1}{k\tau} \epsilon^{-t/\tau} \right) \qquad (4\text{-}21)$$

It is seen that Eq. (4-21) predicts a deviation from a simple exponential decay with a single time constant. The equation should really be applied only in cases where $k\tau \gg 1$. In any event, Eq. (4-21) is in qualitative agreement with the observed experimental behavior of n_e and numerical comparisons are discussed in the next section.

4.IV Computer Calculations

For the purpose of comparison with the simple ambipolar theory [Eq. (4-21)] which becomes inaccurate as the ratio of negative ion to electron concentration becomes large, we obtained some numerical solutions of the equations governing simultaneous diffusion and attachment. The starting point was taken to be the equations

$$\begin{aligned} \frac{\partial n_e}{\partial t} &= D_e \nabla^2 n_e + K_e \nabla \cdot (\underline{E}\, n_e) - k n_e \\ \frac{\partial n_+}{\partial t} &= D_+ \nabla^2 n_+ - K_+ \nabla \cdot (\underline{E}\, n_+) \qquad (4\text{-}22) \\ \frac{\partial n_-}{\partial t} &= D_- \nabla^2 n_- + K_- \nabla \cdot (\underline{E}\, n_-) + k n_e \end{aligned}$$

where free diffusion coefficients are represented by D, mobilities by K, attachment coefficients by k and particle densities by n. The space charge field $\underline{E}$ is determined from Poisson's equation. In the present case, the containing vessel is taken to be an infinite cylinder of radius a. Hence $\underline{E}$ is directed radially and depends only on the distance r from the axis of the cylinder

$$E(r) = \frac{4\pi e}{r} \int_0^r \xi(n_+(\xi) - n_-(\xi) - n_e(\xi)) \, d\xi \qquad (4\text{-}23)$$

where e is the electronic charge. For convenience, we changed to a set of dimensionless parameters defined by

$$R = r/a, \qquad \tau = D_e t/a^2, \qquad N = n/n_o \text{ and } \quad \epsilon = Eae/k_B T$$

n_o being the initial electron density, T the temperature of all species present and k_B the Boltzmann constant. Using the above and the relation $K/D = e/k_B T$ we obtain from Eqs. (4-22) and (4-23)

$$\frac{\partial N_e}{\partial \tau} = \left[\frac{\partial^2}{\partial R^2} + \frac{1}{R}\frac{\partial}{\partial R}\right] N_e + \left[\frac{\partial}{\partial R} + \frac{1}{R}\right](N_e \epsilon) - \frac{ka^2 N_e}{D_e}$$

$$\frac{\partial N_+}{\partial \tau} = (D_+/D_e)\left(\left[\frac{\partial^2}{\partial R^2} + \frac{1}{R}\frac{\partial}{\partial R}\right] N_+ - \left[\frac{\partial}{\partial R} + \frac{1}{R}\right](N_+ \epsilon)\right)$$

$$\frac{\partial N_-}{\partial \tau} = (D_-/D_e)\left(\left[\frac{\partial^2}{\partial R^2} + \frac{1}{R}\frac{\partial}{\partial R}\right] N_- + \left[\frac{\partial}{\partial R} + \frac{1}{R}\right](N_- \epsilon)\right) + \frac{ka^2 N_e}{D_e}$$

$$\epsilon(R) = \frac{4\pi e^2 a^2 n_o}{k_B T} \cdot \frac{1}{R}\int_0^R \eta\left(N_+(\eta) - N_e(\eta) - N_-(\eta)\right) d\eta \qquad (4\text{-}24)$$

For use in the numerical solution of Eq. (4-24) where $\eta = \xi/a$, the discrete variable R(L) was defined as R(L) = L/M where L and M are integers and L = 0, 1, 2, ... M. In other words, the radial distance was divided into M equal parts. Derivatives were calculated at each point R(L) using central difference formulae involving two adjacent points on either side. At R = 0, the expressions $(\partial N/\partial R)/R$ and $(N\epsilon/R)$ are indeterminate but the limits as $R \to 0$ are well defined. A polynomial expression was employed to supply values of the indeterminate

expressions in terms of the values of the same expressions at points near R = 0. A complete cycle of the iteration was then:

(1) obtain $\epsilon(L)$ for each value of L up to M by numerical integration using the existing distributions $N(L,\tau)$

(2) evaluate the derivatives $\partial N/\partial\tau$ at each value of L, using numerical methods for the partial derivatives with respect to R

(3) compute the new particle distributions by applying the formula $N(L, \tau + \Delta\tau) = N(L,\tau) + (\partial/\partial\tau)N(L,\tau)\,\Delta\tau$ at each value of L, for each of electrons, positive ions and negative ions.

For this computation scheme to be stable, there are severe restrictions on the size of the time interval $\Delta\tau$ which can be employed, the maximum $\Delta\tau$ being a function of the initial electron concentration n_o. For M = 20, the maximum usable $\Delta\tau$ ranged from about 8×10^{-4} at $n_o = 10^6$ electrons per cc to 2×10^{-4} at $n_o = 10^8$ electrons per cc.

The value of the diffusion coefficients D_e and D_+ were calculated from available experimental data for 300°K and a pressure of helium of 18 torr. From mobility data for NO^+ in helium,[32] we obtained $D_+ = 20\ cm^2/sec$.

For the electron diffusion coefficient, we employed the formula[33]

$$D_e = \frac{3}{8}\left(\frac{\pi k_B T}{2m^*}\right)^{1/2} \frac{1}{n\sigma}$$

where T is the temperature and k_B is Boltzmann's constant. Electrons are diffusing through the gas with density n molecules per cc and σ is the cross section for this process. m^* is the reduced mass of the electron-molecule pair and is approximately the mass of the electron itself. D_e was computed for a pressure of helium of 18 torr and temperature of 300°K. σ was a momentum transfer cross section for electrons

in helium taken from a paper by Frost and Phelps.[34] We obtained $D_e = 1.0 \times 10^4$ cm^2/sec. Lacking experimental data on the diffusion of the negative ions present, we put $D_- = D_+$. Since the diffusion of negative ions is greatly retarded by the space charge electric field the calculation should not be sensitive to the precise value of D_- selected.

Both total electron concentrations and averages over the TM_{010} electric field [see Eq. (3-13)] were computed. As expected, the decay rates were not sensitive to whether the electron concentrations were averaged or not. Since the electric field average corresponds to the experimentally observable quantity it was used in the analysis. For convenience we list here the fixed parameters in the program.

Diffusion coefficients: $D_e = 10^4$ cm^2/sec

$D_+ = 20$ cm^2/sec

$D_- = 20$ cm^2/sec

cell radius, $a = 1.2$ cm.

cavity radius (for E-field avg.) = 3.5 cm.

From the above, we have $a^2/D_e = 1.44 \times 10^{-4}$ so that 1 unit of program time equals 144 microseconds. As mentioned before, the maximum $\Delta\tau$ was less than 10^{-3} so that considerable time was required on the SDS 910 computer. For this reason, computations were made with the attachment rate constant set at about 10^4 sec^{-1} which corresponds to experimental data for SF_6 and C_7F_{14} where the duration of observed electron decay was only a few hundred microseconds.

A typical computer calculation with $k = 10^4$ sec^{-1} and $n_o = 10^8$ electrons per cc is shown in Fig. 8. The straight line corresponds to

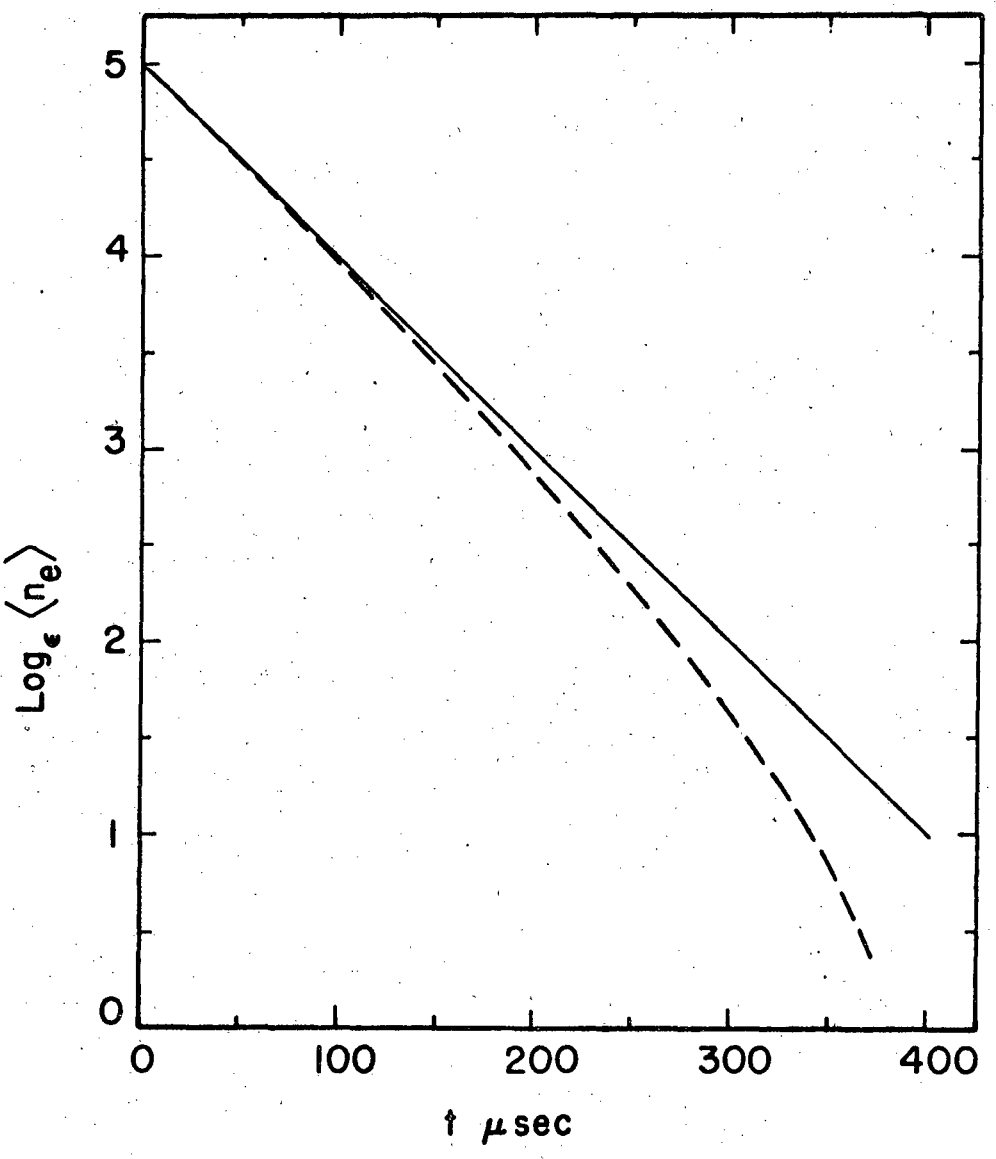

Fig. 8 Electron Decay Curve: Computer Simulation of Attachment and Diffusion for $n_o = 10^8$ electrons/cc, $k = 10^4$ sec^{-1}, Fundamental Diffusion Mode.

purely exponential decay with time constant 10^{-4} sec. The computed curve does not show appreciable deviation from the straight line until the electron concentration has decreased by about an order of magnitude. From this it is apparent that in obtaining slopes from similar experimental data curves emphasis should be placed on points near time t = 0.

A short study of the diffusion of electrons and positive ions in the absence of negative ions was made in order to determine the validity of applying the ambipolar diffusion formulae at various electron concentrations. The initial distribution was selected to give diffusion in the fundamental mode so that the electron concentration as a function of the reduced time and radius parameters, τ and R, should have been

$$N(R,\tau) = J_o(x_{o1}R) \quad \epsilon^{-\left(\frac{D_a}{D_e}\right) x_{o1}^2 \tau} \qquad (4\text{-}25)$$

where J_o is the zero-order Bessel function and x_{o1} its first zero. In practice, it was found that for initial electron concentrations, n_o, of 10^6 or 10^7 per cc noticeable curvature of the computed log $\langle N \rangle$ vs t curve was observed for the first 500 or 300 microseconds, respectively.

This indicates that as t increases in the first few hundred microseconds there is a transition from a fast rate of loss of electrons, corresponding to free diffusion, to a slower rate as a retarding electric field builds up. For $n_o = 10^8$ per cc, straight line behavior of a log $\langle N \rangle$ vs t plot was obtained from times earlier than 20 microseconds. Also, at $n_o = 10^8$ cc^{-1}, the original first mode distribution shape is accurately maintained, whereas at $n_o = 10^7$ or 10^6 cc^{-1} progressively more electrons are lost from the distribution near the wall of the cylinder, leaving the distribution sharply peaked near R = 0. In the following table (Table 2) the effective ambipolar diffusion coefficient,

D_a', was obtained from the slope of a log $\langle N \rangle$ vs t plot at a time t when the plot appeared linear, at least on the time scale employed. D_a was calculated from Eq. (4-12).

Table 2

Effect of initial electron concentration on effective ambipolar diffusion coefficient, D_a'.

n_o electrons/cc	t μ seconds	D_a'/D_a
10^6	1235	5.23
10^7	954	2.02
10^8	173	1.27

It is apparent that straight-line behaviour of a log $\langle N \rangle$ vs t plot over moderate time intervals may correspond to an ambipolar diffusion coefficient somewhat larger than predicted by the simple theory. One of the conditions for the validity of the simple theory is approximate charge neutrality: $(N_+ - N_e)/N_+ \simeq 0$. In fact, for initial electron concentrations of 10^8, 10^7 and 10^6 per cc, the quantity $(N_+ - N_e)/N_+$ evaluated at R = 0 was 2×10^{-4}, 7×10^{-3} and .19, respectively. This indicates that the possibility of simple ambipolar diffusion in the range $10^7 > n_o > 10^6$ cc^{-1} is quite dubious.

Returning to the attachment calculations, we can make some general observations. It appeared that the space charge electric field was established very rapidly after the beginning of computation and thereafter the field varied quite slowly with time. This indicates a steady current of electrons is diffusing to the walls during the attachment run. As

the electron concentration is being reduced by rapid attachment, the fractional loss of electrons by steady diffusion becomes greater as time progresses, giving the behaviour shown in Fig. 8. This qualitative explanation also fits the simple expression (Eq. (4-21)), where the second term is small but decreases more slowly with time than the first term.

The computations showed that with an initially uniform electron distribution the decay rate was a few percent faster than with an initial fundamental-mode distribution. The experimental situation would be expected to be somewhere between these extremes. The following table gives an approximate upper limit to the error in estimating the attachment rate from the slope of the electron decay curve near t = 0. The table applies to an attachment rate, k, of 10^4 sec^{-1}.

Table 3

Error in estimating attachment rates for k = 10^4 sec^{-1}.

n_o electrons/cc	Uniform distribution % error	Diffusion distribution % error
10^6	30-40	30-40
10^7	11	10
10^8	8	4

In practive a correction for diffusion and attachment is obtained from the slope of a log (n) vs t curve for an experiment performed in the absence of the principal attaching gas (see Chapter 5). In the analogous correction for the above computed rates, there is no correction for background attachment but a correction of about 1.6×10^2 sec^{-1}

would be subtracted from k to correct for ambipolar diffusion, thus reducing the error estimates in Table 3 by about 1.6%.

The approximate ambipolar theory and the computer solution for the case: $n_o = 10^8$ cc^{-1}, $k = 10^4$ sec^{-1} and an initial fundamental diffusion mode distribution, were in good agreement for about 400 microseconds, or a decrease in electron concentration by two orders of magnitude. Naturally the simple theory is not accurate in the other cases in Table III since Eq. (4-21) does not predict the effects of varying initial electron concentration and spatial distribution.

5. RESULTS AND DISCUSSION

5.I. Fluorine Compounds

The rate of attachment of thermal electrons to a series of fluorine compounds was studied. Listed in order of decreasing attachment rate, these were SF_6, C_7F_{14}, C_3F_8, C_2F_4, and SiF_4.

It is convenient to discuss the attachment process in terms of the following mechanism.

$$A + e \xrightarrow{k_1} (A^-)^* \qquad (5\text{-}1)$$

$$(A^-)^* \xrightarrow{k_2} A + e \qquad (5\text{-}2)$$

$$(A^-)^* + M \xrightarrow{k_3} A^- + M \qquad (5\text{-}3)$$

where A represents a fluorine-containing molecule and M an inert gas molecule. In the steady state approximation for the unstable negative ion $(A^-)^*$, Eqs. (5-1) to (5-3) give

$$-\frac{1}{n_e}\frac{dn_e}{dt} = \frac{k_1 k_3 [A][M]}{k_2 + k_3[M]} = k \qquad (5\text{-}4)$$

where n_e, [A], [M] are the concentrations of electrons and species A and M, respectively. We have indicated in Eq. (5-4) the relationship of the elementary rate constants k_1, k_2, and k_3 to the first order rate constant k defined in Eq. (4-6). The smallest values of [A] employed were in attachment experiments with SF_6 and C_7F_{14} where pressures of these gases as low as 5×10^{-7} torr were employed. At 300°K, this corresponds to 1.6×10^{10} molecules per cc. Since the initial electron concentration in these experiments was between 10^7 and 10^8 per cc, [A] can be regarded as practically unchanged during the electron

decay.* Hence k in Eq. (5-4) is actually proportional to [A], where we can use the value of [A] at the time the reaction cell was loaded.

As described in detail in Chapter 2, a fixed pressure of NO (about .085 torr) was used in these experiments as a source of photoelectrons. Also, a fixed pressure of helium (about 18 torr) was present to reduce the diffusion rate. Hence, Eq. (5-4) should actually be written

$$-\frac{1}{n_e}\frac{dn_e}{dt} = k + k^* \qquad (5\text{-}5)$$

where k^* includes the contribution to the electron decay rate due to: (i) electron attachment to NO, and (ii) diffusional loss of electrons. Of course, inclusion of the diffusional contribution in this manner is equivalent to assuming that only the fundamental diffusion mode is present (see Chapter 4). This is a good approximation in cases where electron decay was observed over an interval of several milliseconds as was the case for C_3F_8, C_2F_4, and SiF_4. In the case of SF_6 and C_7F_{14}, some higher mode diffusion may have been present during the time when attachment data were being recorded. Here, however, the total correction (including attachment to NO) was in the range 1% to 10% so that the effect, within this correction, of higher mode diffusion can be neglected.

By performing attachment experiments at various pressures of the principal attaching gas, A, and subtracting the correction k^* obtained

---

* There remains the possibility of depleting the supply of attaching gas by repeated flashing of the pulsed lamp. For SF_6, for example, it was observed that by the 100th flash, k had decreased to .6 of its value for the initial flash. For this reason, only data for early flashes were used.

from a similar experiment with no A present, we obtained the first order attachment rate constant k as a function of pressure of A. The results are given in Table 4 and are plotted in Figs. 9-13. Plots were linear and with the exception of the SiF_4 data, could be extrapolated through the origin as expected.

The reason for the anomalous behavior of the SiF_4 data is uncertain. However, it is appropriate to mention the fact that for pressures of C_2F_4 and SiF_4 in the micron range, the attachment rates wereabout the same magnitude as the correction, k^* (k^* was $\sim 4\times10^2$ sec^{-1}). Fluctuations in k^* from one experiment to the next were about 10% of its average value. It was found that heating the reaction cell to about 100°C for several hours between experiments reduced the scatter in the data. This effect was probably associated with outgassing from the cement used to seal the LiF window to the reaction cell. Red glyptal resin proved superior to various epoxy cements in reducing this background attachment.

We considered the use of higher pressures of C_2F_4 and SiF_4 in order to produce a faster electron decay rate thus reducing the relative magnitude of k^*. This was attempted a few times but the values of k obtained were always low when compared with the values expected from extrapolating the low pressure data. The absorption spectra of C_2F_4 and SiF_4 in the vacuum ultraviolet are not known, but it may be that, at the higher pressures, a significant amount of the lamp radiation is absorbed by the C_2F_4 or SiF_4 to produce excited species. The apparent attachment rate in the presence of excited molecules could be diminished because of a competing detachment process.

The lifetime of the excited negative ion produced in process (5-1) is of importance in interpreting the attachment results. In the so-called

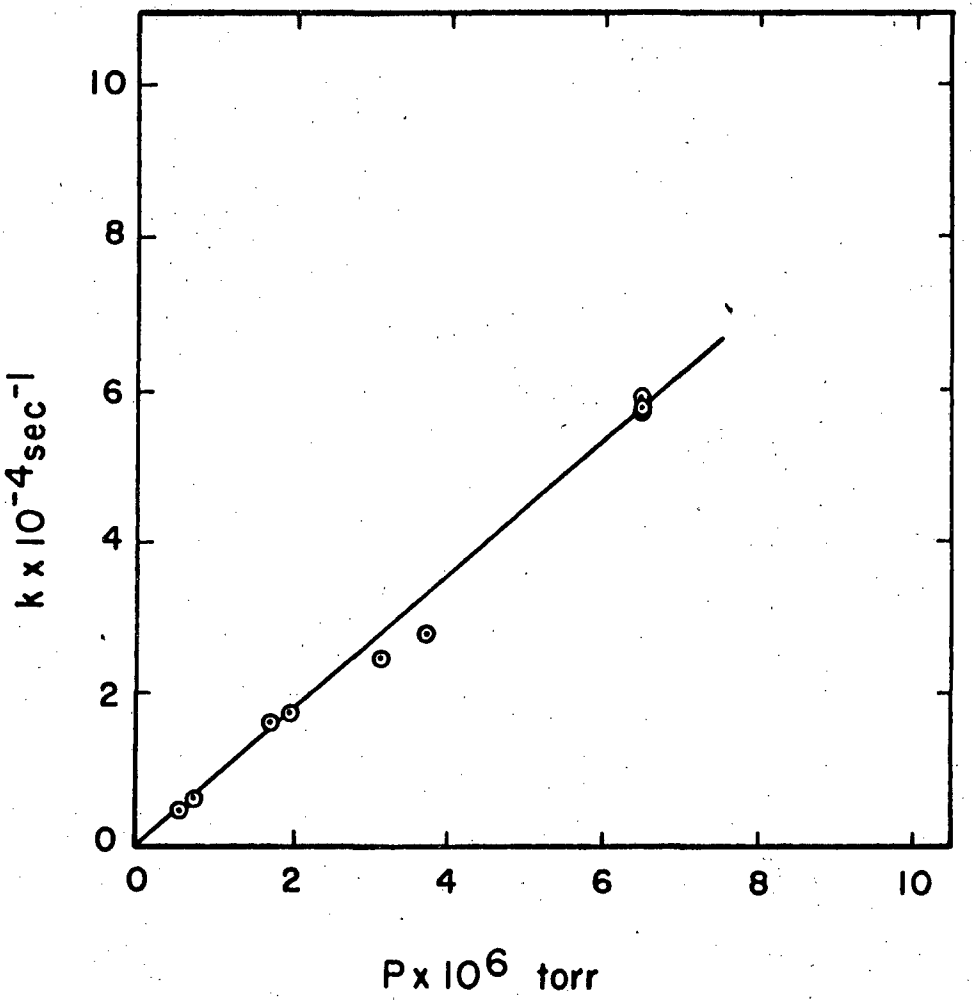

Fig. 9 Pressure Dependence of k: SF_6 Data.

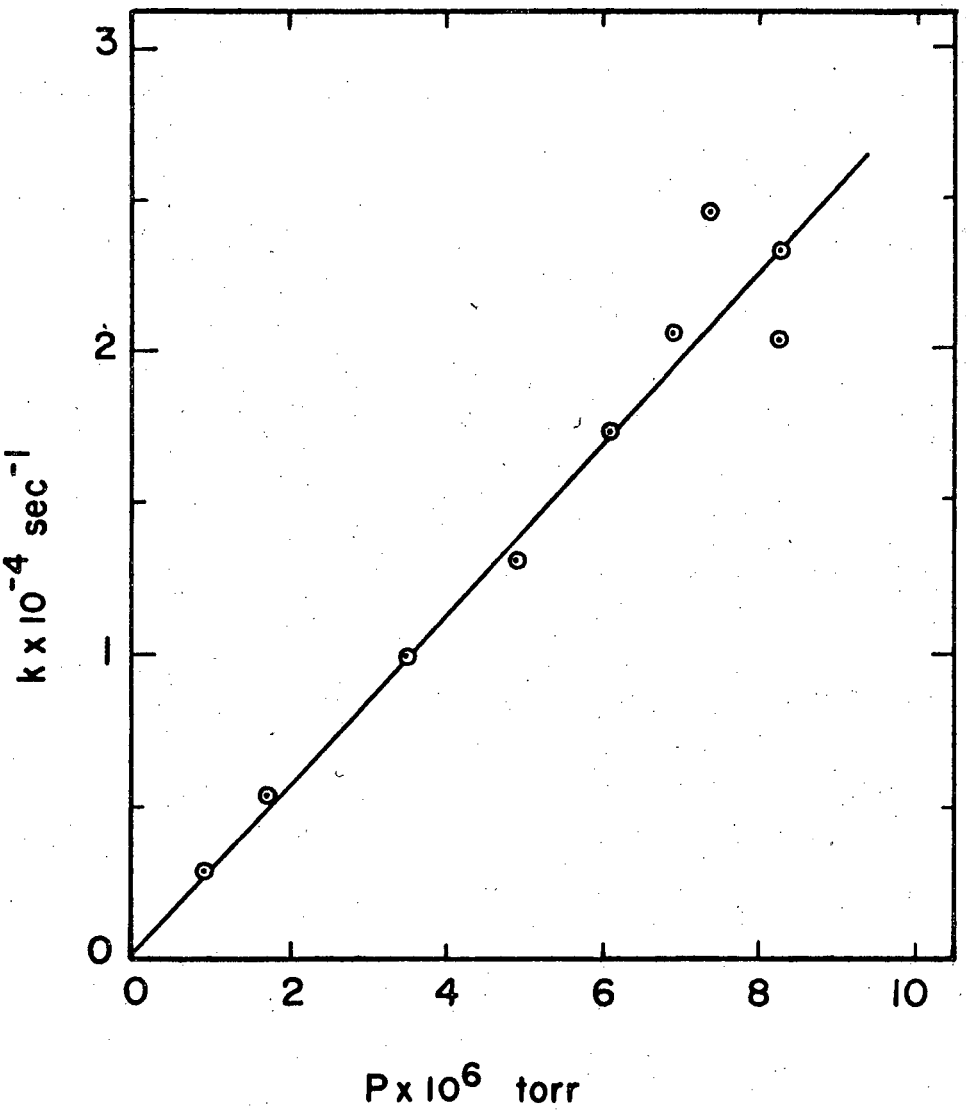

Fig. 10 Pressure Dependence of k: C_7F_{14} Data.

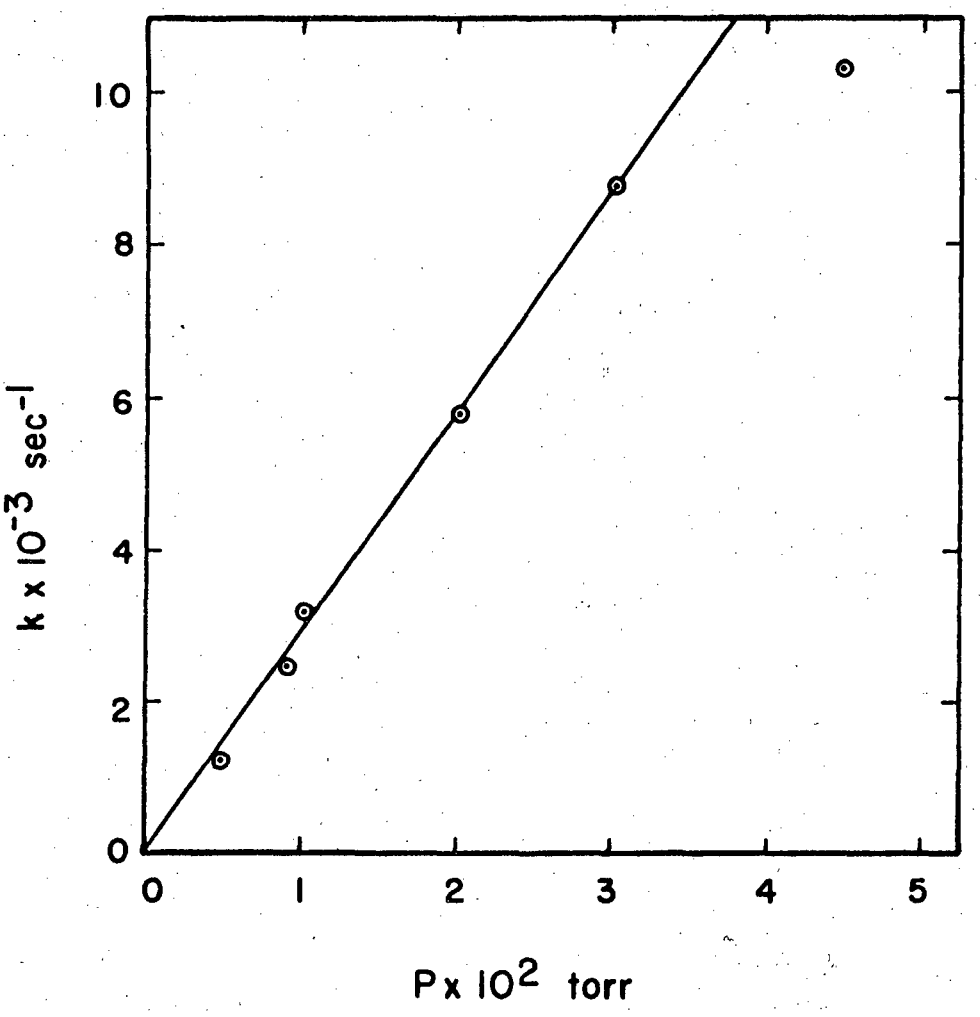

Fig. 11 Pressure Dependence of k: C_3F_8 Data.

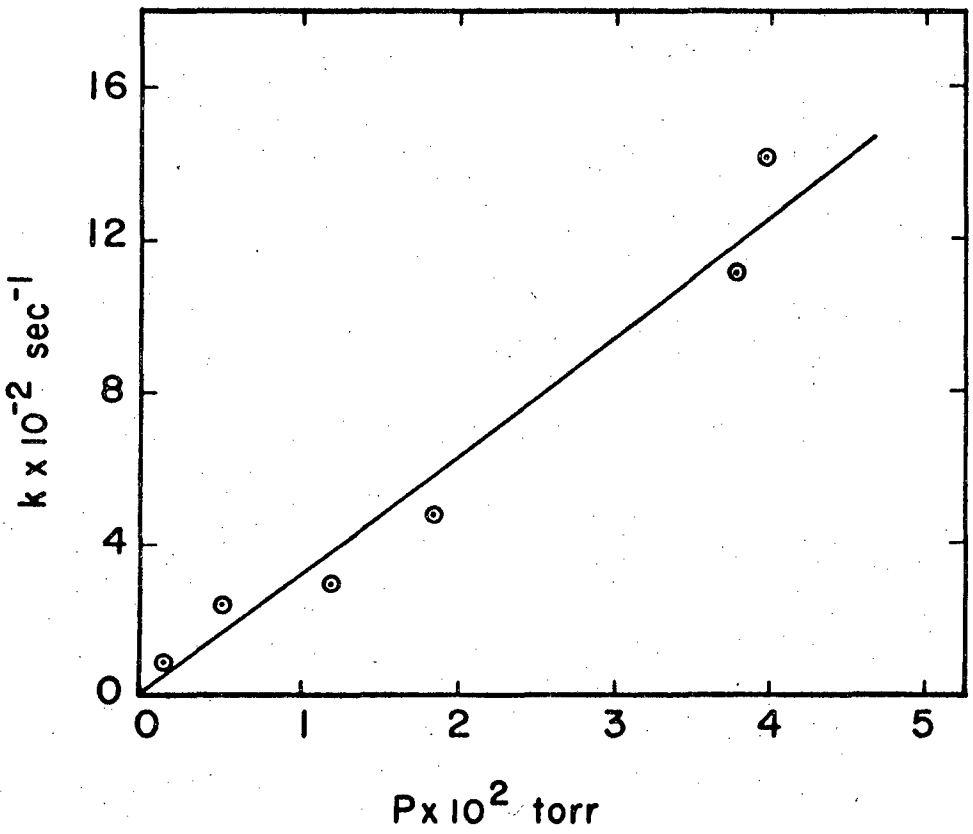

Fig. 12 Pressure Dependence of k: C_2F_4 Data.

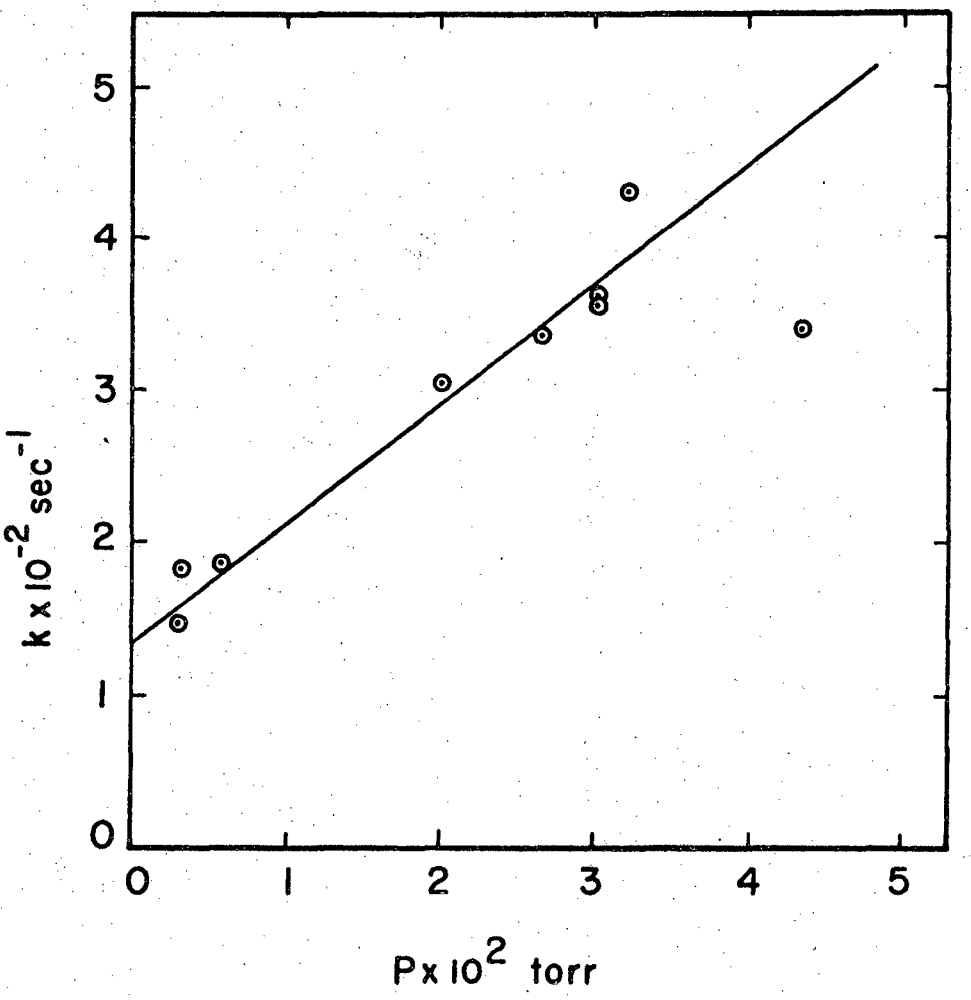

Fig. 13 Pressure Dependence of k: SiF_4 Data.

Table 4. First order rate constants for electron decay.

Pressure SF_6 $\times 10^6$ torr	k $\times 10^{-4}$ sec^{-1}	Pressure C_7F_{14} $\times 10^6$ torr	k $\times 10^{-4}$ sec^{-1}
.55	.44	.97	.29
.68	.55	1.73	.53
1.73	1.55	3.42	.98
1.95	1.74	4.92	1.30
3.12	2.43	6.08	1.72
3.73	2.76	6.91	2.05
6.49	5.64	7.35	2.46
6.49	5.52	8.27	2.03
6.49	5.91	8.27	2.33

Pressure C_3F_8 $\times 10^2$ torr	k $\times 10^{-3}$ sec^{-1}	Pressure C_2F_4 $\times 10^2$ torr	k $\times 10^{-3}$ sec^{-1}
.50	1.22	.15	.083
.82	2.43	.48	.240
1.07	3.14	1.21	.291
2.06	5.79	1.84	.475
3.08	8.77	3.80	1.124
4.52	10.27	3.98	1.514

Pressure SiF_4 $\times 10^2$ torr	k $\times 10^{-2}$ sec^{-1}
.32	1.45
.32	1.82
.58	1.84
2.01	3.04
2.66	3.34
3.02	3.54
3.02	3.60
3.23	4.30
4.37	3.39

"high pressure limit", corresponding to $k_3[M] \gg k_2$ in Eq. (5-4), the excited negative ion is much more likely to undergo a stabilizing collision with an inert gas atom [process (5-3)] than to decompose [process (5-2)]. In that case, the measured rate of electron disappearance is simply the rate for the two-body process (5-1) with rate constant, k_1, given by

$$k_1 = k/[A] \tag{5-6}$$

At the opposite extreme, where decay of the excited negative ion is much more probable than collisional stabilization ($k_2 \gg k_3[M]$, the "low pressure limit"), Eq. (5-4) predicts the attachment rate will be proportional to both [A] and [M]. In that case, we can define a three-body rate constant, k_{3B}, given by

$$k_{3B} = k/([A][M]) \tag{5-7}$$

In intermediate cases, where $k_2 \simeq k_3[M]$, the analysis must involve the complete expression in (5-4) or some similar treatment which involves k_1, k_2, and k_3.

Time-of-flight mass spectrometry[35] has shown that the lifetime of $(SF_6^-)^*$ with respect to process (5-2) is of the order of 10 microseconds. Since the time between collisions in helium at 18 torr is about 10^{-8} seconds, we would expect to be in the "high pressure" region. In fact, variation of the helium pressure in the range 2.6 to 15 torr had no effect on the observed attachment rate to SF_6. We conclude that for SF_6, our experiment measures the two body rate corresponding to process (5-1). The conclusion is the same in the case of C_7F_{14} since the $C_7F_{14}^-$ ion has been observed in a mass spectrometer[36] and must therefore have a lifetime under collision free conditions of at least 10^{-6} seconds.

Mass spectrometric studies[37] of C_3F_8, at pressures of about 10^{-5} torr, have not shown the presence of the $C_3F_8^-$ ion.* However, we observed no variation in k when attachment to C_3F_8 was carried out in neon with the neon pressure varied in the range 2 to 81 torr.

With C_2F_4 and SiF_4, the observed attachment rate showed some dependence on the inert gas pressure, approximately doubling as the inert gas pressure was increased from 10 to 100 torr. As in the study of attachment to NO alone (Section 5.II), the observed electron decay rate, corrected for diffusion, was plotted against inert gas pressure (cf. Fig. 15). Although the C_2F_4 and SiF_4 data showed somewhat more scatter than was present in the NO work, variation of attachment rate with inert gas pressure was definitely present, indicating that attachment to C_2F_4 and SiF_4 should be interpreted as a three-body process.** Analyzing our data in this way, Eq. (5-7) becomes

$$k = (k_{3B}[A] + k'_{3B}[NO])\,[M] \qquad (5\text{-}8)$$

where A is SiF_4 or C_2F_4, k_{3B} and k'_{3B} are three-body rate constants for attachment to A and NO, respectively, and M is the inert gas. We determine k experimentally as a function of [M] for known fixed values of [A] and [NO]. Since we know k'_{3B} from separate experiments with NO,

---

* The ions observed in reference 37 were F^-, CF_3^-, and $C_2F_5^-$ with appearance potentials of 1.8, 2.2, and 2.1 eV, respectively. For thermal electrons, dissociative attachment to $C_3F_8^-$ to form C_3F_7 and F^- seems energetically impossible since the electron affinity of F is 3.448 eV[44] while C-F bond energies are usually in the range 4.4 to 5.2 eV.[41] It is not known, whether dissociative attachment by thermal electrons with the formation of CF_3^- or $C_2F_5^-$ is possible.

** See Appendix

we can calculate k_{3B} from Eq. (5-8). Examples obtained are

C_2F_4 in helium: $k_{3B} = 2\times10^{-30}$ (cc/molecule)^2 sec^{-1}

SiF_4 in helium: $k_{3B} = 3\times10^{-31}$ (cc/molecule)^2 sec^{-1}

A systematic study of the attachment rate to C_2F_4 and SiF_4 as a function of inert gas pressure, for various inert gases, was not carried out. The difficulty in merely obtaining linear plots of the attachment rate as a function of C_2F_4 or SiF_4 pressure has been mentioned previously. This scatter introduces corresponding inaccuracy in the determination of three-body rate constants for these compounds.

In order to compare our data to that available from beam experiments, we require the relation between the attachment rate constant, k_1, and the attachment cross section σ. The required relation is

$$k_1 = \int v(\epsilon)\ \sigma(\epsilon)\ f(\epsilon)\ d\epsilon \qquad (5\text{-}9)$$

where the dependence of the cross section σ, the electron velocity v, and the electron energy distribution function f on the energy of the electron ϵ has been indicated. Here f is normalized to unity. In actual beam studies, the minimum energy spread attainable is typically .1 or .2 eV. By comparison, at 300°K, 90% of the electrons in a Maxwellian distribution have energies between 0 and .08 eV. For this reason, the average cross section defined by $\bar{\sigma}\bar{v} = k_1$, where $\bar{v}$ is the average thermal electron velocity at 300°K, should be a reasonable quantity to compare with the beam results. Our results for k_1 and $\bar{\sigma}$ are given in Table 5.

For comparison, Table 6 lists some results of electron beam studies. We see that there is some disagreement between the values of σ reported and that these values are smaller than our present measurements. This

Table 5. Two body rate constants, k_1, and average cross sections, $\bar{\sigma}$, for electron attachment.

Compound	k_1 $cm^3(molecule\ sec)^{-1}$	$\bar{\sigma}$ cm^2
SF_6	2.7×10^{-7}	2.6×10^{-14}
C_7F_{14}	8.8×10^{-8}	8.2×10^{-15}
C_3F_8	8.8×10^{-12}	8.2×10^{-19}
C_2F_4	(9.4×10^{-13})*	(8.8×10^{-20})*
SiF_4	(2.3×10^{-13})*	(2.2×10^{-20})*

* These numbers result from analyzing the data of Figs. 12 and 13 as a two body process. (In fact, there is probably three-body attachment in these cases -- see text.)

Table 6. Cross section, σ, and electron energy, ϵ_o, at the first maximum in ion current (from electron beam studies).

Compound	σ cm^2	ϵ_o eV	Reference
SF_6	1.3×10^{-15}	.03 ± .03	36
SF_6	5.7×10^{-16}	0.0	59
SF_6	$> 10^{-15}$	.03	38
C_7F_{14}	7.5×10^{-15}	.15	36

can be understood if the cross section for electron capture as a function of energy is a narrow spike with a half-width small compared with the electron beam energy spread. The latter quantity may not be negligible – for example, Hickam and Fox[38] obtained their estimate of 10^{-15} cm^2 for the SF_6 cross section from an assumed energy spread of .05 eV. If the actual capture cross section, $\sigma(\epsilon)$, is large near $\epsilon = 0$ and falls off rapidly with increasing electron energy, we would expect to observe a larger cross section with microwave than with beam methods. This follows from the fact that a Maxwellian distribution is heavily skewed toward low energies, whereas the technique used to produce the electron beam data[3] should give an approximately uniform distribution of electron energies within the energy width of the beam.

In the electron beam studies, it has been noted that the SF_6^- peak has the same shape as a function of the electron energy as does the derivative of electron current from retarding analysis.[38] This evidence supports the conclusion that $\sigma(\epsilon)$ for attachment to SF_6 is very narrow. In our experiments it was observed that if the power of the probing microwave signal was increased by a factor of 30 (thus increasing the temperature of the electron distribution above 300°K) the attachment rate decreased by about 50%. Using Eq. (5-9) we can write, at 300°K

$$\frac{dk_1}{dT} = \frac{d}{dT}\int_0^\infty v(\epsilon)\ \sigma(\epsilon)\ f(\epsilon)\ d\epsilon\ < 0 \qquad (5\text{-}10)$$

where

$$f(\epsilon) = \frac{2\pi}{(\pi k_B T)^{3/2}}\ \epsilon^{1/2}\ \exp(-\epsilon/k_B T)$$

k_B being Boltzmann's constant. If we now assume that $\sigma(\epsilon)$ is a narrow spike of height $\sigma(\epsilon_o)$ and width $\Delta\epsilon$ centered at ϵ_o, condition (5-10)

reduces to

$$\frac{d}{dT}\left(v(\epsilon_o)\ \sigma(\epsilon_o)\ f(\epsilon_o)\right) < 0 \qquad (5\text{-}11)$$

which gives easily

$$\epsilon_o < \frac{3}{2} k_B T \qquad (5\text{-}12)$$

At 300°K this means $\epsilon_o < .04$ eV which is consistent with the value $\epsilon_o = .03$ from beam measurements.[38] The microwave method could be employed for determining ϵ_o very accurately if apparatus were used by which the temperature of the reaction cell could be lowered until $\frac{d}{dT} k_1 = 0$, at which temperature we would have $\epsilon_o = (3/2)k_B T$. A knowledge of ϵ_o for attachment to SF_6 is quite valuable, since it is often used to locate zero on the energy scale in mass spectrometric studies.[39,40]

Within experimental error, variation of probing signal power did not produce observable variation in the attachment rate for any compounds studied other than SF_6. The simplest explanation would be a slow variation of the appropriate cross sections within the accessible electron energy range since then k_1 as given by Eq. (5-9) would be slowly varying with T. This explanation cannot apply to C_7F_{14}, however, since a resonant peak for electron capture has been observed at .15 eV.[36] It seems possible that the true position of the maximum in the capture peak lies closer to the zero of electron energy since otherwise we should have observed an increase in the attachment rate with increase in mean electron energy. Additional evidence for this suggestion is the fact that our observed cross section for electrons of mean energy .039 eV is slightly larger than that given in reference 36 at .15 eV.

5.II. Attachment to NO

In addition to using NO merely as a source of photo electrons in the work on fluorine compounds, we later made some investigations of the process of electron attachment to NO itself. In studies with pure NO, Gunton and Shaw[46] have shown that the electron attachment rate is approximately proportional to the square of the NO pressure thus indicating that attachment to NO is a three body process. In their studies, NO pressures of up to 15 torr at 298°K were employed. With NO alone there is a fairly narrow range over which the pressure can be varied (approximately 3 to 15 torr was used in Ref. 46) since at low pressures, ambipolar diffusion is the dominant process for the disappearance of electrons and at high pressures, the NO strongly absorbs the ionizing 1216 Å radiation. Indeed, the NO photoionization cross section is so large (2.02×10^{-18} cm^2 at 1216 Å)[10] that at 15 torr, 97% of the incident 1216 Å radiation is absorbed in a 3.7 cm path length (the axial length of the cell used in Ref. 46). This gives a very nonuniform initial electron distribution, in contrast to the assumption of axially uniform electron concentration which is used in analyzing the data.

In our experiments, the attachment rate to NO of thermal electrons was studied as a function of the pressure of various inert gases present in the reaction cell. Since these gases do not absorb the 1216 Å radiation, it was possible to go to higher pressures than could be used in reference 46. The lower limit on usuable total pressure is determined by the accuracy with which the observed rate can be corrected for ambipolar diffusion. The upper limit on pressure has to do with the validity of the microwave method when the electron-molecule collision frequency becomes comparable to the radian frequency of the microwave

field (see Section 3.III). Because of this, krypton and xenon were used only up to pressures of about 50 torr whereas with other inert gases pressures of up to 120 torr were employed.

As mentioned in Section 5.I, the electron decay rate in NO fluctuated by about 10% of its average value for different experiments performed under conditions as close to identical as we could achieve. This effect could not be eliminated but could be minimized by mild (100°C) baking of the reaction cell between runs. Higher baking temperatures were not employed because of the softening of the resin used to seal the LiF window to the cell. However, it was noted that the observed electron decay rate, for a given NO and inert gas pressure in the cell, was a slowly varying function of the number of lamp flashes. Typically, the electron decay rate would decrease by less than 10% over the first 10 flashes and more slowly thereafter. Hence it was possible to fill the cell with about .085 torr NO and a few torr of inert gas, flash the lamp a few times and then record a series of electron decay curves, increasing the inert gas pressure between flashes. In this way, we were able to obtain a set of electron decay rates as a function of inert gas pressure without fluctuations in any background attachment rate from one flash to the next. Experimental data obtained this way are given in Table 7.

In discussing the experimental results we wish to consider two possible mechanisms for electron attachment to NO.

Mechanism I:

$$e + NO \xrightarrow{k_1} (NO^-)^* \qquad (5.13)$$

$$(NO^-)^* \xrightarrow{k_2} e + NO \qquad (5.14)$$

$$(NO^-)^* + M \xrightarrow{k_3} NO^- + M \qquad (5.15)$$

Table 7. First order rate constants for electron decay in NO - inert gas mixtures. (P_{NO} = .085 torr)

Run	Buffer Gas	Total Pressure (p) torr	k $\times 10^{-3}$ sec^{-1}	k' $\times 10^{-3}$ sec^{-1}	1/p $torr^{-1}$	$10^3/k'$ sec
2	He	6	.657	.077	.167	13.0
		14	.412	.164	.071	6.10
		25.5	.326	.190	.039	5.26
		45	.313	.236	.022	4.24
		62	.331	.275	.016	3.64
4	Ne	14	.291	.202	.071	4.95
		23.5	.300	.247	.043	4.05
		53	.318	.295	.019	3.39
		81	.345	.330	.012	3.03
		102.5	.390	.378	.010	2.65
6	N_2	7.5	.279	.211	.133	4.74
		16	.280	.248	.063	4.03
		30	.307	.290	.033	3.45
		45	.346	.335	.022	2.99
		72	.443	.436	.014	2.29
		104	.519	.514	.010	1.95
8	Ar	10	.319	.273	.100	3.66
		16	.290	.259	.067	3.86
		25	.325	.306	.040	3.27
		44.5	.357	.347	.023	2.88
		71	.418	.412	.014	2.43
		107.5	.435	.431	.009	2.32
9	Kr	10	.206	.172	.100	5.81
		17	.201	.181	.059	5.52
		27	.198	.185	.037	5.41
		39	.201	.192	.026	5.21
		48.5	.203	.196	.021	5.10
10	Xe	3.1	.374	.294	.323	3.40
		6.5	.330	.292	.154	3.42
		11	.336	.314	.091	3.18
		20	.432	.420	.050	2.38
		35	.573	.566	.029	1.77

Mechanism II:

$$NO + M \xrightarrow{k_1'} NOM \tag{5-16}$$

$$NOM \xrightarrow{k_2'} NO + M \tag{5-17}$$

$$e + NOM \xrightarrow{k_3'} NO^- + M \tag{5-18}$$

In these equations, M refers to the inert gas employed.

In mechanism I, we apply the steady state approximation for the concentration of $(NO^-)^*$ and, representing the diffusion contribution as D_a/Λ_1^2 (see Section 4.III), we obtain for the rate of electron decay

$$-\frac{1}{n_e}\frac{dn_e}{dt} = k = \frac{(k_1 k_3/k_2)[NO][M]}{1 + k_3[M]/k_2} + \frac{D_a}{\Lambda_1^2} \tag{5-19}$$

In mechanism II, we can consider the complex NOM to be in equilibrium with NO and M as given by

$$[NOM] = K\,[NO][M] \tag{5-20}$$

For the cases of interest to us, an estimate of K was made from a calculation based on second virial coefficients described by Hirschfelder and Stogryn.[47] The equilibrium constant K can be calculated from

$$\frac{[NOM]}{[NO][M]} = K = -\frac{4}{3}\pi\sigma^3(B_b^* + B_m^*) \tag{5-21}$$

where B_b^* and B_m^* are second virial coefficients calculated for "bound" and "metastable" pairs in reference 47 using a Lennard-Jones (6-12) potential characterized by the usual parameters ϵ and σ. Tabulated values[45] of ϵ and σ for NO and various inert gases M were combined to produce parameters characteristic of the NO-M interaction using the approximate rules

$$\sigma_{ij} = \frac{1}{2}(\sigma_i + \sigma_j), \qquad \epsilon_{ij} = (\epsilon_i \epsilon_j)^{1/2}$$

where a single subscript refers to the interaction of two molecules of the same type and the double subscript refers to interaction between two different species. Calculated values of ϵ, σ, and K (at 300°K) are given in Table 8. If used to calculate equilibrium constants for bound pairs of like species, K as given by Eq. (5-21) must be divided by 2 (the "symmetry number").

Even though K is small, the condition $n_e \ll [NOM]$ is valid for the small electron concentrations employed in this research, thus justifying the use of the equilibrium value of [NOM] in mechanism II. We can then write

$$-\frac{1}{n_e}\frac{dn_e}{dt} = k = \frac{k_3' K [NO][M]}{1 + K[M]} + \frac{D_a}{\Lambda_1^2} \qquad (5\text{-}22)$$

where [NO] should really refer to the initial concentration of NO, but in practice this quantity does not change measurably either because of NOM formation or electron attachment. An estimate of the diffusional contribution to the electron decay rate in Eq. (5-19) and (5-22) can be made by calculating the ambipolar diffusion coefficient D_a using experimental mobility data. The mobility of a positive ion of mass 30 was obtained by interpolation using reported mobilities of various alkalai metal ions in different inert gases.[48] As described in Section 4.III, we can relate the mobility of the positive ion, K_+, to the corresponding diffusion coefficient, D_+, through the Einstein relation

$$\frac{K_+}{D_+} = \frac{e}{K_B T} \qquad (5\text{-}23)$$

where e is the electronic charge, k_B Boltzmann's constant and T is the temperature in °K. From the additional relations $D_a \simeq 2D_+$ and $\Lambda_1^2 = .248\ cm^2$ (for our cell dimensions) we obtain the first order rate coefficient for electron decay via the fundamental diffusion mode, D_a/Λ_1^2. Since D_+ and therefore D_a show a variation as 1/p where p is the total pressure, the constant quantity $D_a p/\Lambda_1^2$ is given in Table 9. The results of these calculations are in reasonable agreement with experimental measurements for NO^+ where available.[32,49] The diffusion correction is only of comparable magnitude to the attachment rate at the low end of the pressure range employed ($p < 10$ torr) so errors in the calculated diffusion constants cannot affect our conclusions drawn from data taken at medium and high pressures.

Typical data obtained from our experiments are given in Table 7. The total pressure, p, and 1st order electron decay rate constant, k, are the measured quantities. We obtain k' by subtracting a diffusion correction, i.e.,

$$k' = k - \frac{b}{p} \quad \text{where} \quad b = \frac{D_a}{\Lambda_1^2} \tag{5-24}$$

We then write

$$k' = \frac{a[NO][M]}{1 + [M]/c} \tag{5-25}$$

as an appropriate form for comparison with Eqs. (5-19) and (5-22), where a and c are parameters to be determined from the slope and intercept of a plot of 1/k' vs 1/[M]. Actually, for convenience, we plot 1/k' vs 1/p, p being the pressure of inert gas M. The data in Table 7 are plotted this way in Fig. 14. In Table 10 we give the a and c parameters for Eq. (5-25), as determined from the data in Fig. 14 as well as for some

Table 8. Calculated equilibrium constants, K, for weakly bound pairs at 300°K.

Bound Pair	ϵ/k_B °K	σ Å	$-(B_b^* + B_m^*)$	$K \times 10^{23}$ cc/molecule
He-NO	36.6	2.86	.110	1.1
Ne-NO	68.3	2.96	.233	2.5
N_2-NO	111.6	3.43	.488	8.3
Ar-NO	125.3	3.29	.585	8.7
Kr-NO	149.7	3.39	.764	12.4
Xe-NO	170.2	3.64	.906	18.2

Table 9. Correction for ambipolar diffusion, $D_a p/\Lambda_1^2$.

Gas	K_{NO^+} $cm^2\ V^{-1} sec^{-1}$	$D_a p/\Lambda_1^2$ $torr\ sec^{-1}$
He	22.5	3480
Ne	8.	1240
N_2	3.3	510
Ar	3.	463
Kr	2.2	341
Xe	1.6	247

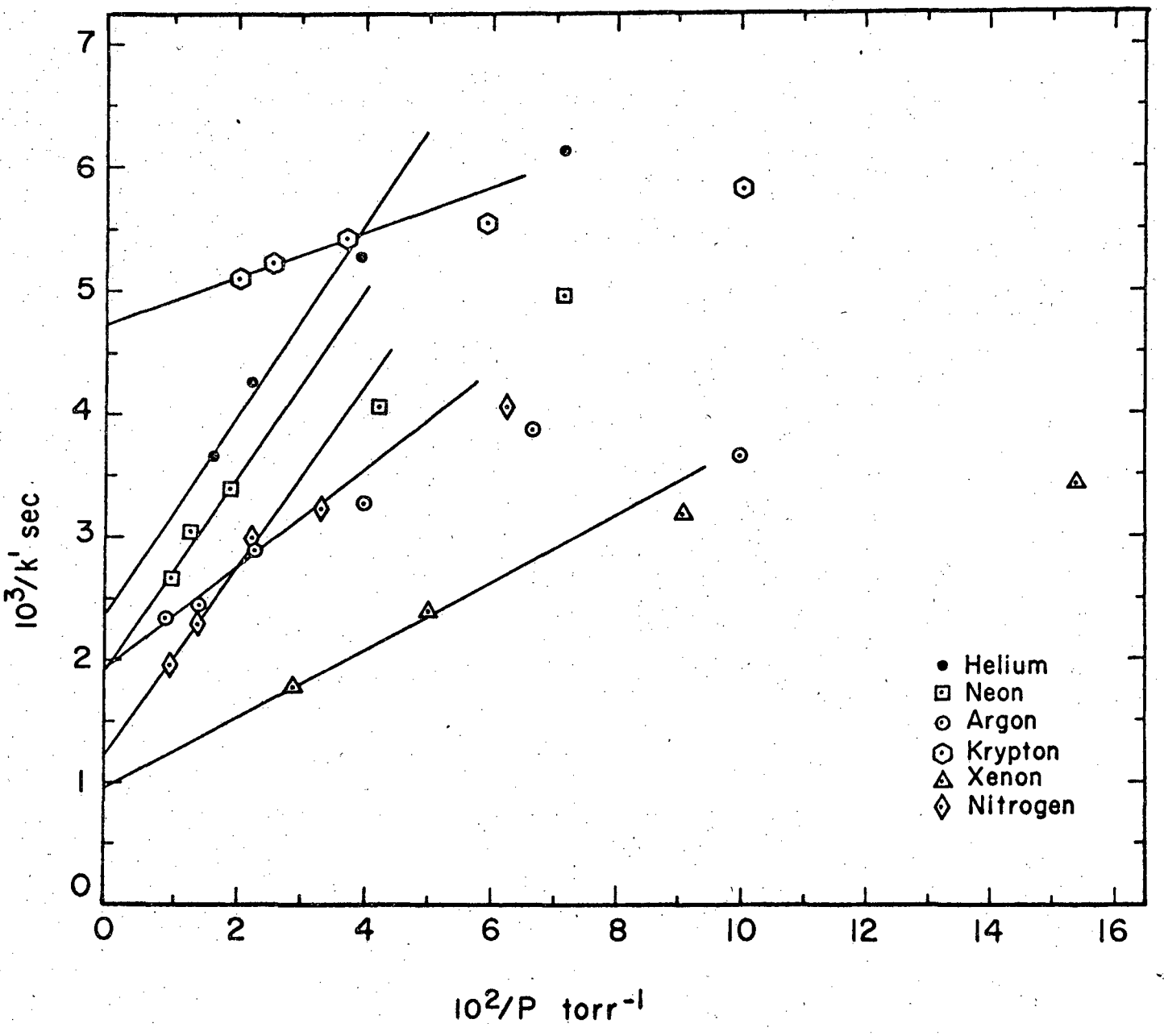

Fig. 14 NO Data: Reciprocal Plots.

additional runs not shown in the figure for clarity.

Another method of analyzing the data is simply to plot k' vs pressure of the inert gas. This corresponds to an attempt to describe the data in terms of a simple three-body attachment mechanism which would predict an equation of the form

$$k' = a' [NO][M] \tag{5-26}$$

It is apparent that this is simply Eq. (5-25) in the "low pressure" limit, i.e., where $[M] \ll c$ in the range of pressures employed. Both mechanisms I and II predict that this is likely to hold, in practice. For example, $[M]/c$ corresponds to $K[M]$ in Eq. (5-22). From values of K in Table 8, we calculate that $K[M] < 10^{-4}$ for pressures of inert gas employed in our studies. Correspondingly, in Eq. (5-19), we need to estimate the ratio $k_3[M]/k_2$. The appropriate arguments for this are most conveniently introduced in Section 5.III where the condition $k_3[M] \ll k_2$ is obtained. There arguments make the use of Eq. (5-26) plausible, at least, and Fig. 15 gives the k' vs p plots for the data in Table 7. (Again, we plot against p rather than [M] for convenience; at 300°K, $[M] = 3.22 \times 10^{16}$ p, where [M] is in molecules/cc and p is in torr.)

It is apparent from Fig. 15 that k varies linearly with inert gas pressure, but the data appears to fit an equation of the form

$$k' = k_a + k_b p \tag{5-27}$$

This could only happen if some electron removal process were present which was independent of inert gas pressure over the pressure range employed. This appears to be the case, however, since Eq. (5-27) appears to give a better fit to the experimental data over the whole range of

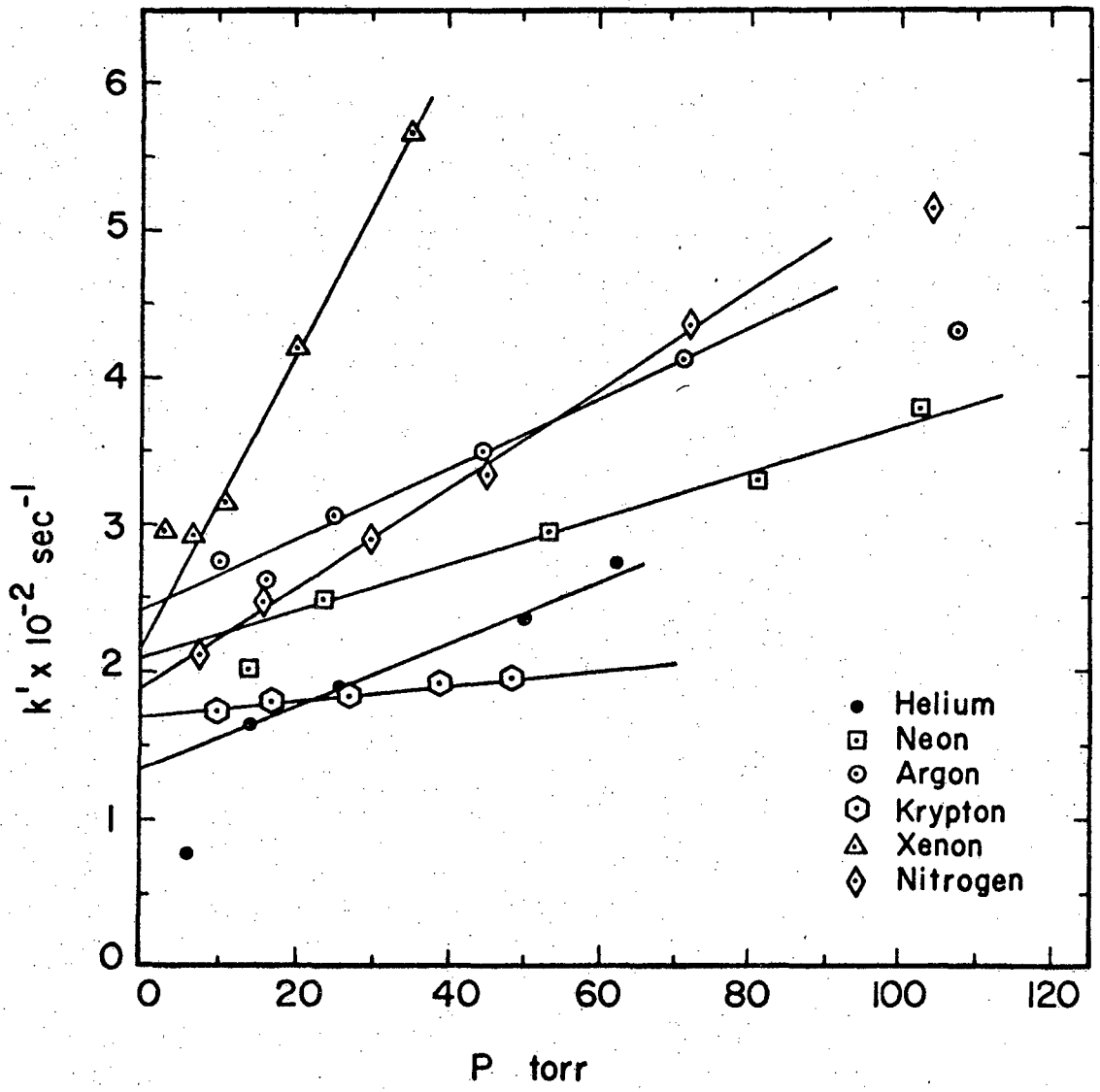

Fig. 15 NO Data: Linear Plots.

pressure studied than does Eq. (5-25). Other considerations favor Eq. (5-27). In particular, the parameter c, obtained from $1/k'$ vs $1/p$ plots (used to evaluate a and c in Eq. (5-25)) turns out to be much smaller than expected with the result that $[M]/c \sim 1$ in the middle of the pressure range employed. This is in severe disagreement with the calculations mentioned above, which predict $[M]/c \ll 1$. It is true that k' decreased slowly as a function of the number of lamp flashes so that the experimental k' values for progressively higher pressure would be too small, but the error involved is only a few percent. Also, in Fig. 14, the data for low pressure falls below the lines extrapolated from high pressure data in all cases. This could be interpreted as being due to a choice of diffusion coefficients which were too small, possibly because the physical situation corresponded to a case intermediate between ambipolar and free diffusion. Such an interpretation does not seem reasonable, however, since Fig. 15 gives no evidence of such a systematic error in the diffusion correction.

The simplest explanation of the above comments is that Eq. (5-27) is indeed the appropriate equation for describing our experimental situation. If this is true, the curvature in Fig. 14 can be explained. For example, $k' = 135 + 2.1\ p\ \text{sec}^{-1}$ gives a good fit to the helium data in Fig. 15. If we now plot $1/k'$ as a function of $1/p$ using

$$1/k' = \frac{1}{135 + 2.1/(1/p)} \qquad (5\text{-}28)$$

the helium data in Fig. 14 is closely reproduced. Equation (5-28) gives a curve which would pass through the origin but the fall off is apparent only at very high pressures (> 100 torr) which were outside the range of our experiments.

The source of the pressure independent attachment rate (giving rise to k_a in Eq. (5-27)) is not apparent. In other experiments, performed with inert gas pressure held constant (at approximately 15 torr), a linear variation of k' with NO pressure was obtained but again with a zero-pressure intercept of about 100 sec^{-1} for k'. Processes which fail to provide an explanation are:

(1) Three body attachment due to NO-NO collisions. The measured three body rate constant at 298°K for this process[46] is 2.2×10^{-31} $(cc/molecule)^2$ sec^{-1} so that at the pressure of NO employed in our inert gas pressure variation experiments (.085 torr) the predicted decay rate is about 100 times smaller than the observed k_a.

(2) Electron-ion recombination. This process gives a decay rate which is second order in electron concentration. At early times in the electron decay process, an "apparent" first order decay rate could be calculated from

$$-\frac{1}{n_e}\frac{dn_e}{dt} = \alpha n_e \qquad (5\text{-}29)$$

Using the recently measured value[49] of α (4.6×10^{-7} cc/sec at 298°K) and a typical initial electron concentration in our experiments (3×10^7 electrons/cc), the predicted decay rate is about a factor of 10 too small to account for k_a.

The finite zero-pressure attachment rate suggests that some impurity may be present in all our NO runs. For example, the vapor pressure of N_2O in equilibrium with solid at 77.3°K is 2.5×10^{-7} torr. If N_2O were released at this pressure during the time the reaction cell was being filled with NO, electron attachment via the process

$$e + N_2O \rightarrow N_2 + O^-$$

might be possible. This process has been observed mass spectrometrically,[53,54] the threshold being for electron energies in the range 0 to .05 eV. If the cross section for dissociative capture of thermal electrons were as large as 10^{-15} cm^2, our observed attachment rate for the limit as inert gas pressure approaches zero could be accounted for.

Actually, it is hard to see how enough N_2O contaminant could be left in the NO supply since repetitive distillation of the NO was performed from a liquid oxygen bath (p_{N_2} = 5.6×10^{-5} torr, p_{NO} = 3.22 torr) to a liquid nitrogen bath. It does not seem likely that N_2O was produced by photolysis.[11] However it seems likely that some impurity exhibiting a two body attachment rate was present. This question cannot be considered resolved.

Three body rate constants a' [Eq. (5-26)], calculated from the slopes of plots such as Fig. 15, are given in Table 10. Because of arguments given in this section, we consider these results more likely to be correct than the corresponding quantities a, calculated from 1/p plots and Eq. (5-25).

5.III Detailed Comparison of Mechanisms

We shall start this section by focusing attention on step [Eq. (5-15)] of mechanism I. The electron affinity of NO has been experimentally determined as .9 eV[50] (more recent evidence indicates it may be closer to .4 eV[51]) hence $(NO^-)^*$ probably refers to a molecular ion in a low vibrationally excited state. In that case, the magnitude of the rate constant k_3 depends on the effectiveness in removing vibrational excitation of collisions of the excited ion with other molecules in the gas. Information from studies on vibrationally excited diatomic molecules

Table 10. Parameters from analysis of attachment rates for NO [Eqs. (5-27) and (5-27)].

Run	Buffer Gas	$a \times 10^{31}$ $(cc/molecule)^2 sec^{-1}$	$c \times 10^{-18}$ cc^{-1}	$a' \times 10^{32}$ $(cc/molecule)^2 sec^{-1}$
1	He	1.1	1.1	2.0
2	He	1.4	1.0	2.3
3	Ne	2.0	0.5	1.5
4	Ne	1.5	1.3	1.8
5	Ne	1.3	1.5	2.0
6	N_2	1.5	1.9	3.7
7	Ar	3.3	0.8	3.7
8	Ar	2.7	0.7	2.6
9	Kr	6.3	0.1	0.65
10	Xe	3.9	0.9	11.0
11	Xe	2.8	1.3	9.5

shows that the probability of deactivation per collision, P_{10}, is quite small. For example, Callear[52] has studied the vibrational relaxation of NO in mixtures with several gases. Values of P_{10} were 3.55×10^{-4} for NO-NO collisions and 4×10^{-7} for NO-N_2 collisions. It was found that in krypton and helium the vibrational relaxation of NO was slightly slower than in N_2, indicating that perhaps a vibrational exchange process was involved in the latter case. Other small diatomic species generally show a smaller deactivation probability for collisions with molecules of the same type than does NO. For example, from data in the literature[43] we conclude that P_{10} for pure oxygen, carbon monoxide and nitrogen at 300°K is 10^{-8}, $< 3 \times 10^{-10}$ and $< 10^{-9}$, respectively. We also note that, for a given molecule, the vibrational deactivation probability generally decreases with increasing mass of the colliding partner (provided chemical affinity is not a consideration). For example, at 291°K for Cl_2, the deactivation efficiencies, relative to collision with another Cl_2 molecule, of collision with H_2, He, and N_2 are 44, 38, and .8, respectively.[43]

In view of the experimental data, it is probably not an overestimate to place the deactivation probability per collision as about 10^{-6} in process (5-15). We can than place an upper limit on $k_3[M]$, where we write $k_3 = \sigma_3 v_3$, σ_3 being the cross section for process (5-15) and v_3 the relative speed of $(NO^-)^*$ and M. Writing σ_3 as the product of a typical gas kinetic cross section multiplied by the deactivation probability we estimate $k_3 = 10^{-15} \times 10^{-6} \times 10^5$ cc/sec or at ~ 30 torr inert gas pressure, $k_3[M] \simeq 10^2$ sec^{-1}. By comparison, k_2 in Eq. (5-14) is the reciprocal of the collision free lifetime of $(NO^-)^*$ which cannot be more than a few vibrational periods. As estimate of k_2 might be 10^{13} sec^{-1}. We see that the condition $k_2 \gg k_3[M]$ seems to be

adequately satisfied. This estimate has been referred to in Section 5.II.

Using Eqs. (5-19) and (5-22), we can compare, approximately, the rates predicted by mechanisms I and II. We have

$$\frac{k'_I}{k'_{II}} \simeq \frac{(k_1 k_3/k_2)[NO][M]}{Kk'_3[NO][M]} = \frac{k_1 k_3}{k_2 k'_3 K} \tag{5-30}$$

We now write $k_1 = \sigma_1 v_1$, $k_3 = \sigma_3 v_3$, $k'_3 = \sigma'_3 v'_3$, where the v's and σ's refer to the relative speeds and cross sections, respectively, involved in the various collisions [processes (5-13), (5-15), and (5-18)]. Certain of these quantities can be estimated at once. We have, as order of magnitude estimates, $v_1 = v'_3 = 10^7$ cm/sec, $v_3 = 10^5$ cm/sec, $K = 10^{-23}$ cm^3 and, from our previous estimate $\sigma_3 = 10^{-21}$ cm^2. Thus

$$\frac{k_1 k_3}{k_2 k'_3 K} = 10^{-6} \left(\frac{\sigma_1}{\sigma'_3}\right) \tag{5-31}$$

Both σ_1 and σ'_3 are cross sections for electron-molecule collisions with formation of negative ions, the latter case involving a dissociation. If these cross sections are comparable, the rate predicted by mechanism I is smaller than the rate for mechanism II by about the value of the deactivation probability we employed for process (5-15). If we assume σ'_3 is about 10^{-15} cm^2 we have via mechanism II

$$k' \simeq 10^{-31} [NO][M] \tag{5-32}$$

For NO pressure of 0.1 torr and inert gas pressure p torr, Eq. (5-32) gives, approximately $k' = 10\ p\ sec^{-1}$ which is comparable with observed electron decay rates. According to this argument, mechanism I could not give decay rates fast enough to agree with our experimental observations.

The observed trend towards higher three body rate constants for heavier inert gas species is further evidence suggesting that mechanism II is preferable. Mechanism I would predict decreasing three body attachment rate constants as a function of mass of M since that is the mass dependence of the vibrational deactivation involved in step (5-15). On the other hand, for the loosely bound species NOM, the equilibrium constant increases from He-NO to Xe-NO, so that mechanism II predicts the observed trend in three body attachment rate constants. In this latter argument, we have ignored the possibility that a variation with M in the equilibrium radius of NOM could produce a shift in the crossing point for the potential energy curves which correspond to NO^- + M and NO + M (+ free electron) at infinite NO-M separation. This could have an appreciable effect on the cross section for dissociative attachment, σ_3'. Some such effect may be responsible for the anomalous behavior of krypton, although there is no data to confirm this.

In the last few years, various workers have measured three body rate constants for thermal electron attachment to NO[46] (third body: NO) and to O_2 [55,56,57,58] (third bodies used: O_2, N_2 and He). These rate constants, k_{3B}, are given in Table 11 for comparison with our own data (averages of a' from Table 10) listed there. It is seen that in producing electron attachment to NO, NO itself is about twice as effective as Xe and ten times as effective as He, as a third body. The variation in effectiveness of third bodies is even greater in the case of attachment to O_2, He being 100 times less effective than O_2. The mechanism involved in electron attachment in pure oxygen has been discussed by Chanin et al.[55] along lines similar to our discussion of NO. It was concluded that the data did not indicate a clear choice between a

Table 11. Third body dependence of the rate of electron attachment to NO and O_2 at 300°K.

Bound Pair	$K \times 10^{23}$ cc/molecule	$k_{3B} \times 10^{32}$ $(cc/molecule)^2 sec^{-1}$	$\sigma_3' \times 10^{16}$ cm^2	Ref.
NO-He	1.1	2.2	1.8	*
NO-Ne	2.5	1.8	.65	*
NO-N_2	8.3	3.7	.41	*
NO-Ar	8.7	3.2	.34	*
NO-Kr	12.4	.65	.05	*
NO-Xe	18.2	10.3	.51	*
NO-NO	4.2	22.	4.8	46
O_2-O_2	4.9	280.	52.	55
		240.	45.	56
		230.	43.	57
		210.	39.	58
O_2-N_2	9.1	15.	1.5	57
		11.	1.1	58
		5.	.5	55
		3.5	.35	56
O_2-He	1.2	2.8	2.1	55

* This research

mechanism involving dissociative attachment to a loosely bound O_4 complex and an alternate mechanism involving vibrational deactivation of excited O_2^- ions. There were difficulties with each interpretation; in the former case, the attachment rate should have increased with a decrease in temperature, which was not observed, and in the latter case, the vibrational stabilization cross section which would have to be assumed to explain the observed rates was very large (10^{-14} cm^2).

In the second column of Table 11, we give equilibrium constants for the formation of loosely bound dimers, calculated as described in Section 5.II from Eq. (5-21). From the equations

$$k_{3B} = k_3' K = \sigma_3' v_3' K \qquad (5\text{-}33)$$

we can get an estimate of σ_3', which is the cross section for the formation of negative ions by dissociative capture (process (5-18)). Using a value of 1.1×10^7 cm/sec for v_3', the relative velocity of electron and molecule, we obtain the estimate of σ_3' given in Table 11. For NO-M, we see that σ_3' appears to go through a minimum as the mass, M, of the third body increases. This could represent some systematic variation with M of the relative positions of the NO-M and $(NO\text{-}M)^-$ potential energy curves, although we lack information for a detailed consideration of this point.

It should be noted that all the values we calculate for σ_3' are reasonable in that they are less than corresponding gas kinetic collision cross sections, except for the case corresponding to attachment in pure oxygen. However, this may be evidence that the mechanism involving the vibrational deactivation of O_2^{-*} ions by O_2 molecules may be applicable in this case. Otherwise, the attachment mechanism involving loosely bound molecular complexes seems quite feasible.

APPENDIX

The observed inert gas pressure dependence of electron attachment to C_2F_4 and SiF_4 indicates that the condition $k_2 > k_3$ [M] must hold in Eq. (5-4). We can think of process (5-3) as being similar to the deactivation of a vibrationally excited polyatomic molecule, whereas process (5-2) is the spontaneous ejection of an electron from an excited ion. We wish to see whether a reasonable upper limit on the electron affinity of the fluorine-containing molecule can be obtained using our observation $k_2 > k_3$ [M].

For k_2, we take the statistical approach of Kassel[42] and write

$$k_2 = A\left(\frac{N(E-E_o)}{N(E)}\right) \qquad \text{(A-1)}$$

where A is a frequency factor and N(E) is the total number of vibrational states for energy 0 to E. In Kassel's theory, the molecule was considered equivalent to s weakly coupled harmonic oscillators, with the dissociation process of interest taking place if energy E_o or greater were present in a critical oscillator. Thus N(E) was the sum of vibrational states up to energy E for a systems of s-1 oscillators. In our case, we can assume that the electron must possess a minimum energy E_o to be ejected from the excited negative ion. This would leave energy $E-E_o$ to be spread amongst s modes of vibration of the molecule.

For an estimate of N(E) for s oscillators, some possibilities are

Classical,[60] $$N(E) = \left(\frac{E^s}{s!}\right) \Big/ \prod_i^s (h\nu_i) \qquad \text{(A-2)}$$

Semiclassical,[61] $$N(E) = \frac{(E+E_v)^s}{s!} \Big/ \prod_i^s (h\nu_i) \qquad \text{(A-3)}$$

$$\text{Modified Semiclassical,}^{62} \quad N(E) = \frac{(E + aE_v)^s}{s!} \Big/ \prod^{s} (h\nu_i) \qquad (A\text{-}4)$$

In the above, E_v is the zero-point vibrational energy of the system of s oscillators with frequencies ν_i. In Eq. (A-4), a is a dimensionless parameter (dependent on E) of the order of unity, calculated for each specific molecule of interest to give a better approximation to its actual vibrational state distribution. Using Eqs. (A-2), (A-3), and (A-4) in Eq. (A-1), we obtain for k_2 the expressions (A-5), (A-6) and (A-7), respectively.

$$k_2 = A\left(\frac{E-E_o}{E}\right)^s \qquad (A\text{-}5)$$

$$k_2 = A\left(\frac{E-E_o+E_v}{E+E_v}\right)^s \qquad (A\text{-}6)$$

$$k_2 = A\left(\frac{E-E_o+aE_v}{E+aE_v}\right)^s \qquad (A\text{-}7)$$

We can write $E = E_T + E_A$ and $E_o = E_A$ where E_T is the average thermal energy of a gaseous electron and E_A is the electron affinity of the molecule.

Taking SiF_4 as an example, we put $A = 10^{13}$ sec^{-1} and $s = 9$. We take E_v equal to its value for the neutral species (0.359 eV)[62] and also calculate a for neutral SiF_4. Values of k_2 calculated from Eqs. (A-5) to (A-7) are given below.

	$k_2(sec^{-1})$		
E(eV)	(A-5)	(A-6)	(A-7)
0.2	4.1×10^{6}	4.7×10^{11}	1.4×10^{11}
0.5	1.1×10^{3}	9.9×10^{9}	1.9×10^{9}
1.0	2.1×10^{-1}	1.6×10^{8}	2.4×10^{7}
1.5	5.4×10^{-2}	9.5×10^{6}	1.4×10^{6}
2.0	4.1×10^{-3}	1.1×10^{6}	1.6×10^{5}

We now wish to obtain an estimate of the magnitude of $k_3[M]$ for SiF_4 to compare with k_2. Provided the electron affinity of the SiF_4 molecule is small, the excited molecular ion will be in a low vibrational state. In such a case, data in the literature on vibrational deactivation times is relevant. Data for SiF_4 is unavailable, but CF_4 has a relaxation time of about 8×10^{-7} sec at 300°K and 1 atmosphere pressure.[43] Using tabulated molecular radius parameters[45] we calculate the collision frequency for a CF_4 molecule as 6.5×10^{9} sec^{-1} at atmospheric pressure so that we can say the vibrational deactivation probability per CF_4-CF_4 collision is about 2×10^{-4}. The deactivation probability depends on the nature of the species colliding with the vibrationally excited CF_4 molecule. Experimental data[43] show that a collision with a helium atom is a factor of 10 more effective than a collision with another CF_4 molecule in producing vibrational deactivation. For neon and argon, the corresponding factors are 2.5 and 0.6. Using this data we obtain $k_3[M]$ as the product of a vibrational deactivation probability and gas kinetic collision frequency. For a few microns of CF_4 in 20 torr of inert gas (typical conditions for our experiments) we calculate

CF_4-M

M	Collision frequency (sec^{-1})	$k_3[M]$ (sec^{-1})
He	3.4×10^8	0.7×10^6
Ne	1.8×10^8	0.9×10^5

In comparing k_2 with $k_3[M]$ we use the more reliable estimates corresponding to Eqs. (A-6) and (A-7), which differ greatly from the classical estimate (A-5), which is known to be poor for small $E-E_o$. If our estimates of $k_3[M]$ based on a small vibrational deactivation probability are correct, the condition $k_2 > k_3[M]$ will hold for electron affinities up to about 2eV. For such a high value of E_A, the negative ion may be in a high enough vibrational state so that deactivation may be expected on nearly every collision. This increases $k_3[M]$ and thus lowers our estimate of the upper limit on E_A into the range 0.5 to 1.0 eV.

It must be admitted that in the above calculation we have applied simple statistical ideas and have not given a detailed model for the ejection of an electron by an excited negative ion. Nevertheless, the limit obtained for the electron affinity is quite reasonable and does not conflict with our experimental observation of three body attachment to SiF_4 and C_2F_4.

ACKNOWLEDGMENTS

This research was directed by Professor Bruce H. Mahan, whose helpfulness at every stage of the investigation is hereby gratefully acknowledged.

This research was performed under the auspices of the United States Atomic Energy Commission to whom my thanks are due for support. I am also grateful to the Woodrow Wilson Fellowship Foundation and the University of California for fellowships in the academic years 1963-1964 and 1965-1966.

REFERENCES

1. R. E. Fox, W. M. Hickam, T. Kjeldaas, J. D. Grove, Phys. Rev. 84, 859 (1951).
2. L. M. Chanin, A. V. Phelps, M. A. Biondi, Phys. Rev. Letters, 2, 344 (1959).
3. R. E. Fox, W. M. Hickam, T. Kjeldaas, J. D. Grove, Rev. Sci. Instr., 26, 1101 (1955).
4. L. G. H. Huxley, R. W. Crompton, The Motion of Slow Electrons in Gases in Atomic and Molecular Processes (Academic Press, New York, 1962).
5. M. A. Biondi, Rev. Sci. Instr. 22, 500 (1951).
6. H. Margenau, Phys. Rev. 69, 508 (1946).
7. M. A. Biondi, Phys. Rev. 109, 2005 (1958).
8. R. E. Nightingale, A. R. Downie, D. L. Rotenberg, B. Crawford, Jr., R. A. Ogg, Jr., J. Phys. Chem. 58, 1047 (1954).
9. H. L. Johnston, W. F. Giauque, J. Am. Chem. Soc., 51, 3194 (1929).
10. K. Watanabe, J. Chem. Phys. 22, 1564 (1954).
11. A. G. Leiga, H. A. Taylor, J. Chem. Phys. 42, 2107 (1965).
12. H. Margenau, Phys. Rev. 73, 297 (1948).
13. L. M. Hartman, Phys. Rev. 73, 316 (1948).
14. A. D. MacDonald and S. C. Brown, Phys. Rev. 75, 411 (1949).
15. A. D. MacDonald and S. C. Brown, Phys. Rev. 76, 1634 (1949).
16. W. P. Allis and S. C. Brown, Phys. Rev. 87, 419 (1952).
17. H. Margenau, Phys. Rev. 109, 6 (1958).
18. E. A. Desloge, S. W. Matthysse, and H. Margenau, Phys. Rev. 112, 1437 (1958).
19. L. S. Taylor, Phys. of Fluids 4, 1499 (1961).

20. W. P. Allis, Handbuch der Physik, Vol. 21.

21. See, for example, Chapman and Cowling, The Mathematical Theory of Non-Uniform Gases, (Cambridge University Press, 1960), p. 46.

22. J. B. Hasted, Physics of Atomic Collisions, (Butterworths, 1964), p. 11.

23. H. J. Oskam, Phillips Res. Repts. 13, 335 (1958); 13, 401 (1958).

24. See, for example, Moreno, Microwave Transmission Design Data, (Dover, 1958).

25. T. M. Shaw, G. H. Brooks, and R. C. Gunton, Rev. Sci. Instr. 36, 478 (1965).

26. J. C. Slater, Rev. Mod. Phys. 18, 441 (1946).

27. R. V. Pound, Rev. Sci. Instr. 17, 490 (1946).

28. K. B. Persson, Phys. Rev. 106, 191 (1957).

29. A. V. Phelps, O. T. Fundingsland, and S. C. Brown, Phys. Rev., 84, 559 (1951).

30. H. S. W. Massey and E. H. S. Burhop, Electronic and Ionic Impact Phenomena (Oxford University Press, 1952), p. 279.

31. E. W. McDaniel, Collision Phenomena in Ionized Gases, (John Wiley and Sons, 1963), p. 512.

32. R. A. Young, C. R. Gatz, R. L. Sharpless, C. M. Ablow, Phys. Rev., 138, A359 (1965).

33. R. D. Present, Kinetic Theory of Gases, (McGraw-Hill Book Co., 1958), p. 55.

34. L. S. Frost, A. V. Phelps, Phys. Rev. 136, A1538 (1964).

35. D. Edelson, J. E. Griffiths, and K. B. McAffee, Jr., J. Chem. Phys., 37, 917 (1962).

36. R. K. Asundi and J. D. Craggs, Proc. Phys. Soc. (London), 83, 611 (1964).

37. M. M. Bibby and G. Carter, Trans. Faraday Soc., 59, 2455 (1963).

38. W. M. Hickam and R. E. Fox, J. Chem. Phys. 25, 642 (1956).

39. R. E. Fox and R. K. Curran, J. Chem. Phys. 34, 1595 (1961).

40. D. C. Frost and C. A. McDowell, J. Chem. Phys. 29, 964 (1958).

41. V. I. Vedeneyev, L. V. Gurvich, V. N. Kondvat'yev, V. A. Medvedev, and Ye. L. Frankovich, Bond Energies, Ionization Potentials and Electron Affinities (St. Martins, 1966).

42. L. S. Kassel, J. Phys. Chem. 32, 225 (1928).

43. A. W. Read, Vibrational Relaxation in Gases, in Progress in Reaction Kinetics (Pergamon Press, 1965), Vol. 3.

44. R. S. Berry and C. W. Reimann, J. Chem. Phys. 38, 1540 (1963).

45. J. O. Hirschfelder, C. F. Curtiss, and R. B. Bird, Molecular Theory of Gases and Liquids, (John Wiley and Sons, 1954), Table I-A.

46. R. C. Gunton and T. M. Shaw, Phys. Rev. 140, A748 (1965).

47. J. O. Hirschfelder and D. A. Stogryn, J. Chem. Phys. 31, 1531 (1959); see Errata in J. Chem. Phys. 33, 942 (1960).

48. S. C. Brown, Basic Data of Plasma Physics (MIT Press, 1959), p. 78.

49. R. C. Gunton and T. M. Shaw, Phys. Rev. 140, A756 (1965).

50. A. L. Farragher, F. M. Page, and R. C. Wheeler, Discussions Faraday Soc. 37, 203 (1964).

51. A. V. Phelps, private communication.

52. A. B. Callear, Discussions Faraday Soc. 33, 61 (1962); see also N. Basco, A. B. Callear, and R. W. Norrish, Proc. Roy. Soc. A260, 459 (1960); and Proc. Roy. Soc. A269, 180 (1962).

53. R. K. Curran and R. E. Fox, J. Chem. Phys. 34, 1590 (1961).

54. G. J. Schulz, J. Chem. Phys. 34, 1778 (1961).

55. L. M. Chanin, A. V. Phelps, M. A. Biondi, Phys. Rev. 128, 219 (1962).

56. J. J. Lennon, M. J. Mulcahy, Proc. Phys. Soc. 78, 1543 (1961).

57. R. Hackam, J. J. Lennon, Proc. Phys. Soc. 86, 123 (1965).

58. V. A. J. VanLint, E. G. Wikner, D. L. Trueblood, Bull. Am. Phys. Soc. 5, 122 (1960).

59. I. S. Buchel'nikova, Zh. Eksperim. i Teor. Fiz. 35, 1119 (1958); (English translation: Sov. Phys. JETP 8, 783 (1959)).

60. R. C. Tolman, The Principles of Statistical Mechanics (Oxford University Press, 1938) p. 492.

61. R. A. Marcus and O. K. Rice, J. Phys. and Colloid Chem. 55, 894 (1951).

62. G. Z. Whitten and B. S. Rabinovitch, J. Chem. Phys. 38, 2466 (1963).